

## Review

# Transforming Energy with Single-Atom Catalysts

Shipeng Ding,<sup>1</sup> Max J. Hülsey,<sup>1</sup> Javier Pérez-Ramírez,<sup>1,2,\*</sup> and Ning Yan<sup>1,\*</sup>

**Almost a quarter of the energy consumed globally is directly or indirectly related to the use of a catalytic process. Conventional nanoparticle-based catalysts recently witnessed the dawn of its potential successor—heterogeneous single-atom catalysts (SACs), which allow the maximum possible dispersion of metal atoms on the catalyst surface, possess unparalleled electronic structure and geometric configuration, and exhibit, otherwise, exceptional performance in a range of energy-related applications. Herein, we critically review the use of heterogeneous SACs in the generation and conversion of hydrocarbons, oxygenates, H<sub>2</sub> fuel, ammonia, commodity and fine chemicals, and the electrochemical energy storage in and release from batteries. We describe the importance of those energy-related compounds in the current energy infrastructure and discuss how catalysis—in particular, single-atom catalysis—can be used more effectively in each application. At last, general guidelines and trends guiding the future design of stable and efficient single-atom catalysts for sustainable energy transformations are provided.**

## Introduction

Ever since the beginning of the twentieth century, the demand for energy and technological advances have been intercorrelated with the rapid development of new processes for the conversion of different forms of energy. The development and expansion of the car generated the increased demand for the liquid instead of previously dominant solid fuels. Most fractions of crude oil, the only abundant resource of liquid energy carriers, however, are not suitable for combustion in engines. Following the demand of lower molecular weight products, thermal cracking, the decomposition of longer into shorter hydrocarbons was developed. If a solid acid catalyst is added, the reaction can occur at significantly lower temperatures, and the selectivity to fuels with a higher octane number is increased. Catalysts, therefore, act by facilitating the overall reaction as well as favoring certain products, resulting in the reduced energy consumption of the process. This and other closely related catalytic processes nowadays are used to produce almost all available petrol, jet, and diesel fuels. Beyond hydrocarbon cracking, catalytic materials have been used for a variety of reactions such as the Haber-Bosch process for the fixation of atmospheric nitrogen, the production of hydrogen from natural gas, the synthesis of plastics, and commodity and fine chemicals—most of which rely on the use of metallic transition metals on metal oxides.<sup>1</sup>

As shown in Figure 1A, the energy consumption based on nuclear and coal resources are not expected to increase any further in the next few decades. The demand for petroleum and other liquid fuels will continue to increase in the upcoming decades while renewable resources and natural gas, both of which are much more directly related to catalysis than nuclear energy and coal, are projected to play a dominant role by 2050. It becomes apparent that the industrial sector is currently responsible

## Context & Scale

Energy cannot be created or destroyed; rather, it can only be transformed or transferred from one form to another. As such, catalysis, an essential tool to manipulate the chemical transformations of energy by the “bond breaking-bond forming” principle, profoundly shapes the landscape of the energy sector. Single-atom catalysts (SACs) featuring atomically dispersed metal atoms on a support recently emerged as a new frontier in catalysis and have achieved encouraging progress in the applications of energy conversion. In this review, six key areas are highlighted where advancements in the SAC research benefit the efficient transformation of energy. Those areas are categorized by hydrocarbon, oxygenate and H<sub>2</sub> fuels, electrochemical energy storage, the production of ammonia, and the less-energy-intensive production of chemicals. Emphasis is given to the utilization of renewable energy sources.

This Review also points out where the remaining opportunities are. To save cost and ensure element sustainability, more effort should be devoted to 3d metals like Fe, Co, Ni, and Cu. If SACs are ever to be used in large scale, reliable and scalable synthetic procedures to make high metal-loading SACs



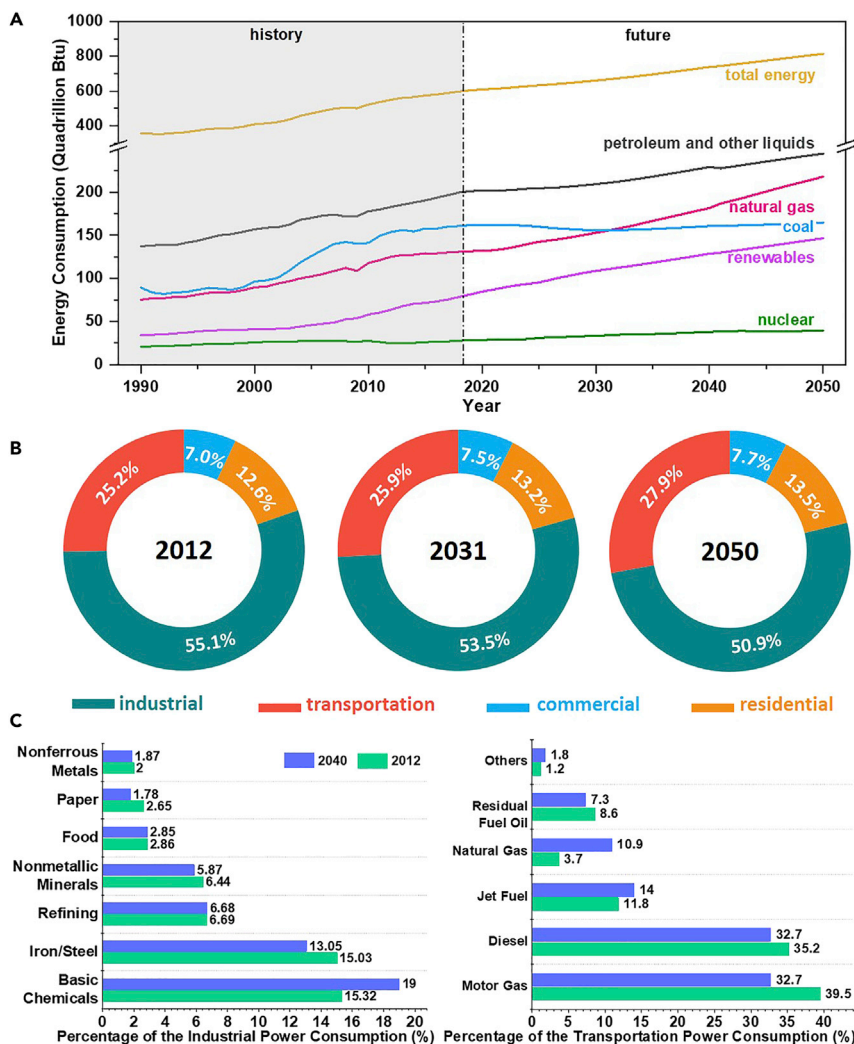


**Figure 1.** Previous, Current, and Projected Energy Consumption by Energy Source, Sectors and Subsectors

(A) Global energy consumption by energy source.

(B) Energy consumption by sector in the years 2012, 2031 and 2050.

(C) Energy consumption by subsector in the years 2012 and 2040. Data obtained from EIA.<sup>2–4</sup>

for more than half of the global energy consumption, with a projected slight decrease of 4.2% in 2050 (Figure 1B). Similarly, the transportation sector accounts for around another quarter of the global energy consumption and will moderately rise. The commercial and residential energy consumption makes up less than 25% in 2012, and will continue to be less than a quarter by 2050. When taking a closer look at the energy consumption of industrial subsectors (Figure 1C), catalysis-related processes such as the production of basic chemicals will witness an overall growth in significance until 2040. The same trend is obvious for the transportation subsectors with an obvious increase in the use of natural gas and jet fuels whereas the consumption of diesel and motor gas are projected to plummet.<sup>2–4</sup> Despite its already high significance in current energy-related industries, we expect catalytic processes to grow in importance in the future for the utilization of both conventional and unconventional energy resources. In particular, a number of above-mentioned chemical transformations have already become active research topics in SAC.

that are stable under industrially relevant conditions are crucial. New techniques that not only image metal species but also differentiate more active sites from less- and non-active ones are highly desired. SACs must be developed for other potentially more challenging energy-related transformations like the Fischer-Tropsch or crude oil cracking reactions. The emerging synergy between machine learning and high-throughput experimentation should be fully exploited to expand the space of SACs relevant for energy application. Improved theoretical protocols should be developed to simulate the catalytic reactions under realistic conditions and establish generalizable scaling relations. To bridge the gap between single-atom and nanoparticle catalysts, an atom-by-atom approach to synthesize active sites ranging from isolated atoms to well-defined metal clusters is needed.

<sup>1</sup>Department of Chemical and Biomolecular Engineering, National University of Singapore, 4 Engineering Drive, Singapore 117585, Singapore

<sup>2</sup>Institute for Chemical and Bioengineering, Department of Chemistry and Applied Biosciences, ETH Zurich, HCI E125, Vladimir-Prelog-Weg 1, 8093 Zurich, Switzerland

\*Correspondence: [jpr@chem.ethz.ch](mailto:jpr@chem.ethz.ch) (J.P.-R.), [ning.yan@nus.edu.sg](mailto:ning.yan@nus.edu.sg) (N.Y.)

<https://doi.org/10.1016/j.joule.2019.09.015>

Reports on atomically dispersed ionic transition metals have been reported earlier.<sup>5–11</sup> Then the term “single-atom catalysis” (SAC) was coined in 2011 by Zhang, Li, Liu, and colleagues, and has spurred tremendous developments. The evolution of related concepts and name conventions have been detailed recently,<sup>12</sup> and herein, we will focus the scope of this review predominantly on energy-related applications published in the recent decade.<sup>13</sup> Comprehensive introduction on the synthetic strategies of SACs,<sup>14–16</sup> specific types of support materials,<sup>17–19</sup> electrocatalysis,<sup>16,18,20</sup> and photocatalysis<sup>21,22</sup> could be found in excellent reviews that were recently published. In contrast to nanoparticle-based catalysts, where a significant fraction of metal atoms is buried below the surface and is thus inaccessible to reactants, SACs offer the maximum possible atom economy and maximized metal-support interactions. SACs exhibit electronic states ranging from positively to negatively charged and carry the absence of neighboring metallic atoms, significantly different from metallic nanoparticles. Furthermore, nanoparticles tune properties through d-band, while SACs display unique tunability because of their homogeneous-like ability to control the frontier orbital geometry and energy of the active sites. Meanwhile, the geometric structures of SACs are also different from that of homogeneous catalysts.<sup>23</sup> The metal species of homogeneous catalysts are coordinated by ligands or substrates. The geometric structures are flexible and the coordination environment can be changed easily during the reaction conditions. For single-atom catalysts, the geometric structures are partially restricted by the support, which could be regarded as a rigid, bulky ligand to coordinate single-atom metals. Those unparalleled properties give rise to unique reactivity patterns and have thus enabled their potential use in a range of energy applications.<sup>12,16,24</sup>

Figure 2 depicts the conversion of energy carriers, in particular, fossil resources such as natural gas, crude oil, and coal as well as renewable energy such as solar, wind, hydro, and biomass over SACs. The products of those reactions might be the final products, or represent energy carriers that are used for grid-scale or transportation-scale energy storage including hydrocarbon, oxygenate, hydrogen, and ammonia fuels as well as a variety of chemicals and electrochemical energy storage systems. Each of those sectors will be reviewed and assessed individually in the context of SAC, and a general future perspective for the field of SAC for energy applications will be provided.

### Hydrocarbon Fuels

Hydrocarbon fuels are currently produced from fossil fuels (coal, petroleum, and natural gas).<sup>25</sup> They are likely to remain as the principal sources of transportation fuels for the next decades. According to the International Energy Outlook 2017 released by the U.S. Energy Information Administration, the world primary fossil fuels consumption reached 514 quadrillion Btu in 2017, accounting for 82% of the global primary energy consumption. The global fossil fuels consumption is projected to reach 739 quadrillion Btu in 2040. Due to the diminishing fossil fuel reserves and continuous increase in CO<sub>2</sub> emission from human activity, it becomes desirable to develop efficient catalytic systems to produce hydrocarbon fuels from sustainable resources such as biomass and CO<sub>2</sub>.<sup>26</sup>

#### Biomass to Hydrocarbons

As the most abundant renewable organic carbon source, biomass is an attractive alternative feedstock for fuels. In many developing countries, a large percentage of fuels consumed is derived from biomass.<sup>27</sup> The transformation of oxygen-rich biomass to hydrocarbon fuels requires oxygen removal reactions such as hydro-deoxygenation (HDO) to form molecules that have desirable properties for

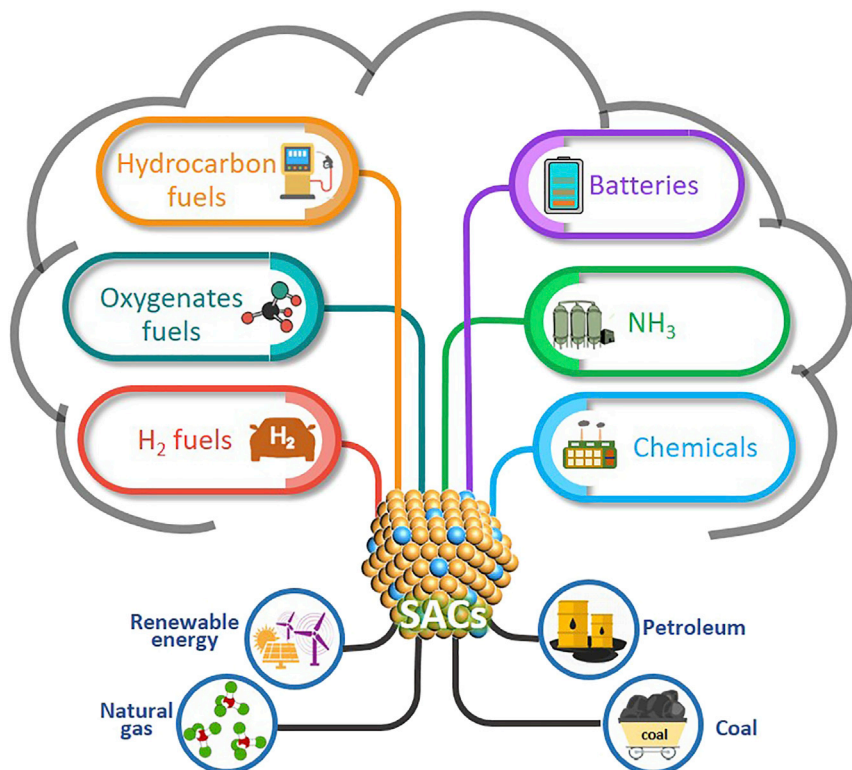


**Figure 2. Overview of the Use of Single-Atom Catalysts (SACs) for Energy Conversions and Savings, the Production of Chemicals and Materials**

upgrading. The traditional HDO catalysts generally suffer from poor catalytic performance and fast deactivation at high temperature. To improve the activity and stability of HDO catalysts, Tsang and co-workers developed a single-atom Co/MoS<sub>2</sub> catalyst, in which isolated Co atoms were anchored covalently to sulfur vacancies of MoS<sub>2</sub> monolayers.<sup>28</sup> The single Co atoms were observed in the HAADF-STEM images (Figure 3A), and DFT calculation was carried out to simulate the geometric structure of Co (Figure 3B). The prepared Co/MoS<sub>2</sub> catalyst with a large number of Co-S-Mo active sites exhibited excellent performance in the selective HDO of lignin-derived 4-methylphenol to toluene. The high catalytic performance of Co/MoS<sub>2</sub> allowed the reaction to proceed at 180 °C, which normally requires 300 °C to occur. The lower operation temperature triggers energy saving, as heating is one of the main costs in large-scale industry applications, potentially pushing the hydrocarbon fuels production from biomass to commercial viability. Later, Tsang and co-workers designed a bifunctional catalyst consisting of atomically dispersed Pd and ultrasmall molybdenum phosphate nanoparticles for the conversion of phenolic monomers as well as wood and bark-derived oligomers into liquid hydrocarbons.<sup>29</sup> The prepared catalyst showed almost complete conversion of phenol to cyclohexane at 383 K. It was proposed that atomically dispersed Pd species promoted the hydrogenation of phenol to cyclohexanol, which was dehydrated to cyclohexene by Brønsted and Lewis acid sites on MoO<sub>3</sub>-P<sub>2</sub>O<sub>5</sub> nanoparticles. Finally, the formed cyclohexene was hydrogenated to cyclohexane. The bifunctional catalyst also displayed state-of-the-art activity for the production of hydrocarbon fuels from water-insoluble bio-oil with a yield of 29.6 wt % under mild conditions.

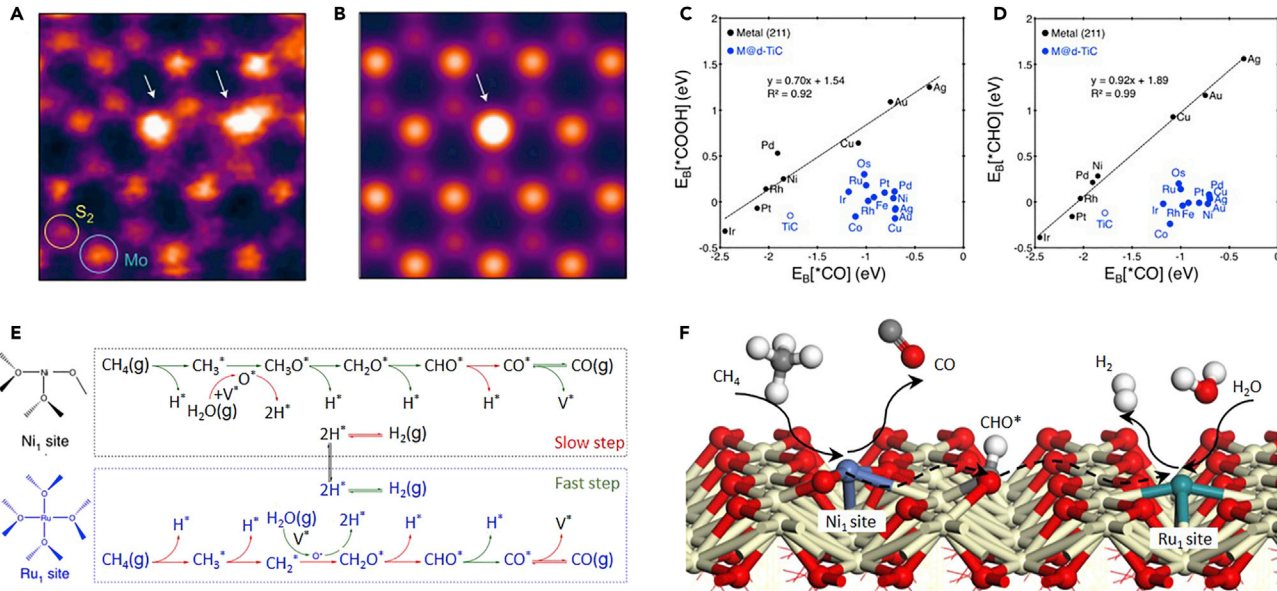


**Figure 3. SACs for the Production and of Oxidation of Hydrocarbon Fuels**

(A and B) HAADF-STEM image of single-atom Co/MoS<sub>2</sub> (A) and HAADF image simulation by DTF (B).

Reprinted from Stang et al.,<sup>28</sup> with permission. Copyright 2017, Nature Publishing Group.

(C and D) \*COOH (C) and \*CHO (D) binding energies as a function of \*CO binding energy for transition-metal (211) surfaces (black) and M@d-TiC (blue). Blue hollow circles represent binding energies on the TiC(100) surface. Reprinted from Jun et al.,<sup>39</sup> with permission. Copyright 2017, American Chemical Society.

(E and F) The proposed reaction mechanism for the conversion of CH<sub>4</sub> to CO on Ni sites and activation of H<sub>2</sub>O on Ru sites. The kinetically favorable and unfavorable steps are marked with green and red arrows, respectively. Cerium, carbon, oxygen, and hydrogen atoms are shown in yellow, gray, red and white, respectively.

Reprinted from Liu et al.,<sup>54</sup> with permission. Copyright 2018, Nature Publishing Group.

### CO<sub>2</sub> to Hydrocarbon Fuels

The production of hydrocarbon fuels from CO<sub>2</sub> reduction may both mitigate global climate change and secure energy supply, but one shall keep in mind that every step for the transformation of CO<sub>2</sub> needs energy, including capture, storage, and conversion. The cost of capturing CO<sub>2</sub> from the air was estimated to range from \$94 to \$232 per ton of CO<sub>2</sub>.<sup>30</sup> The advancement of techniques is likely to further bring down the cost to make CO<sub>2</sub> a viable carbon source. In parallel, a cheap and renewable energy source such as electricity or H<sub>2</sub> is needed to upgrade CO<sub>2</sub>. Another critical issue is to develop highly active catalysts that are able to lower the reaction temperature and pressure without compromising activity, thus decreasing the energy consumption. Besides, catalysts with excellent selectivity would avoid the energy-intensive separation and purification process. Recent studies suggest that SACs are promising catalysts for CO<sub>2</sub> transformation into hydrocarbons.

The desirable CO<sub>2</sub> reduction pathway is the direct one-step conversion into hydrocarbons and oxygenates (vide infra). Most of the currently available catalysts, however, can only reduce CO<sub>2</sub> to CO, which is the first step towards the production of hydrocarbon fuels,<sup>31</sup> but recent advances suggest SACs might be exceptional. SACs showed tunable selectivity towards CO<sup>32–34</sup> and hydrocarbons.<sup>35</sup> Single atoms Pt/Pd supported on g-C<sub>3</sub>N<sub>4</sub> for the photocatalytic reduction of CO<sub>2</sub> was studied using DFT calculation by Du and co-workers.<sup>36</sup> In the presence of Pt or Pd single atoms, the absorption edge of g-C<sub>3</sub>N<sub>4</sub> was extended from 2.7 to 0.2 eV as a result of the electron excitation from d band of the metal to the conduction band of g-C<sub>3</sub>N<sub>4</sub>.

For Pd<sub>1</sub>/g-C<sub>3</sub>N<sub>4</sub>, HCOOH is the favored product with an activation barrier of 0.66 eV; however, Pt<sub>1</sub>/g-C<sub>3</sub>N<sub>4</sub> preferred the formation of CH<sub>4</sub> with a barrier of 1.16 eV. Head-Gordon and co-workers further examined *in silico* the electrocatalytic reduction of CO<sub>2</sub> to hydrocarbons on 28 single-atom alloys (SAAs), in which single-atom M species (M = Cu, Ni, Pd, Pt, Co, Rh, and Ir) were dispersed on the host Au or Ag.<sup>37</sup> The SAAs with M = Co, Rh and Ir, showed desirable performance in the conversion of CO<sub>2</sub> to methane. It was calculated that the host metals Au or Ag were responsible for the reduction of CO<sub>2</sub> to CO, which was captured and further converted to methane by the nearby single-atom species. The performance of transition metals in CO<sub>2</sub> electrocatalytic reduction was limited by the scaling relationship.<sup>38</sup> To break it, Jung and co-workers studied the catalytic performance of TiC as well as single metal atoms doped-TiC during CO<sub>2</sub> hydrogenation by DFT.<sup>39</sup> As shown in Figures 3C and 3D, the binding energy of both \*COOH and \*CHO on pure metals depends linearly on the binding energy of \*CO; however, a nonlinear relationship was observed on TiC-supported SACs. These calculations offer encouraging motivation to develop and characterize SACs for CO<sub>2</sub> conversion. The theoretical calculation predicted that single-atom Cu dispersed on the CeO<sub>2</sub> (110) surface could induce the formation of three oxygen vacancies in each neighboring Cu atom, and promote the conversion of CO<sub>2</sub> to methane.<sup>40</sup> Experimental results were consistent with the prediction that an excellent selectivity towards CH<sub>4</sub> was achieved on mesoporous CeO<sub>2</sub> nanorod supported single-atom Cu species.

In 2016, Ye and co-workers reported an efficient single-atom Co catalyst supported on porphyrin-based MOF for the conversion of CO<sub>2</sub> to CH<sub>4</sub> under visible light, mimicking the photosynthetic process in nature.<sup>35</sup> Both experiment and theory demonstrated that atomically dispersed Co atoms improved the electron-hole separation efficiency in the metal-organic framework (MOF). The photogenerated electrons were transferred efficiently from MOFs to single Co atoms. Compared with the MOF without Co, the incorporation of single-atom Co to MOF increased the formation rate of CH<sub>4</sub> by up to 6 times.

#### Methane to Ethane, Ethylene, and Aromatics

Methane is the main component of natural gas. According to the U.S. Energy Information Administration, the global methane consumption was 130 quadrillion Btu in 2017, and is projected to rise to 218 quadrillion Btu in 2050.<sup>2–4</sup> Around 90% of global natural gas production is used in the direct combustion for electricity generation and industrial heating,<sup>41</sup> and less than 1% natural gas is being used as transportation fuels in the U.S.<sup>42</sup> Industry is interested in the transformation of natural gas to easily transportable vehicle fuels such as aromatics and higher-value compounds to reduce the need for coal and petroleum.<sup>43</sup> Both indirect and direct strategies for the conversion of methane to higher hydrocarbon fuels have been explored.<sup>44</sup> The indirect methods require the formation of syngas (a mixture of H<sub>2</sub> and CO), which is then transformed to hydrocarbons by Fischer-Tropsch synthesis. Syngas production is an energy-intensive process, accounting for over 60% of the total capital cost of gas to liquid plants.<sup>45</sup> The direct transformation of methane circumvents the low efficiency and high capital cost syngas production step, although it suffers from severe thermodynamics limitations at low temperature.<sup>46,47</sup>

In 2014, Bao and co-workers reported the direct methane conversion to higher hydrocarbon products in oxygen-free conditions at high temperature.<sup>48</sup> Single-atom Fe embedded in the silica matrix (Fe/SiO<sub>2</sub>) exhibited 48.1% methane conversion, and 99% total hydrocarbon (such as ethylene and aromatics) selectivity at 1,090°C in a single pass experiment. No coke deposition was detected due to the absence

of adjacent Fe species, which are considered necessary for oligomerization. In 2018, the nonoxidative conversion of methane to higher hydrocarbons was also reported on single-atom Pt/CeO<sub>2</sub> catalysts at 900–1,000°C,<sup>49</sup> and the onset temperature of methane activation (less than 900°C) was a bit lower than that over Fe/SiO<sub>2</sub> (less than 950°C). It was also demonstrated that, under mild conditions, single-atom Rh/ZrO<sub>2</sub> was efficient for the conversion of methane to ethane by O<sub>2</sub> in the gas phase, while only CO<sub>2</sub> was formed over Rh nanoparticles.<sup>50</sup> The stabilization of CH<sub>3</sub> intermediates over single-atom Rh was crucial for methanol and ethane formation, while the C–H bonds of adsorbed CH<sub>3</sub> species were successively dissociated on Rh nanoparticles. Although the conversion of methane was limited, this work opens up a new way for the production of value-added fuels from methane under mild condition.

#### Oxidation of Methane in Fuel Cell

Apart from making higher hydrocarbons, the conversion of methane in fuel cells using SACs has been demonstrated. Compared to the conventional combustion-based technologies, fuel cells are able to convert the chemical energy of the fuels to electricity with less pollution and higher efficiency. Although H<sub>2</sub> is the most ideal energy source in fuel cells, the cheaper and more readily available hydrocarbon fuels such as methane are more attractive in the immediate future. The potential of using hydrocarbon fuels in the solid oxide fuel cells (SOFCs) has been investigated, either via the direct electrochemical oxidation of hydrocarbons or via formation of H<sub>2</sub> and CO as the first step.<sup>51,52</sup> However, the extremely high operating temperature (800–1,000°C) hampered the practical application of hydrocarbon fuel-cells.<sup>53</sup> It is desirable to develop hydrocarbon fuel cells working at intermediate temperature.

Along this line, Liu and co-workers reported a robust methane fuel cell, in which a catalyst with atomically dispersed Ru and Ni on CeO<sub>2</sub> was coated on the anode.<sup>54</sup> The fuel cells enabled the direct electrochemical oxidation of methane containing 3.5% H<sub>2</sub>O at 500°C with no apparent coke formation after operation for 550 h. The authors attributed the outstanding activity and stability to the synergistic effect of single-atom Ni and Ru species in activating methane and H<sub>2</sub>O. As shown in Figures 3E and 3F, DFT simulations showed that single-atom Ni is responsible for the activation of C–H bond in methane. To form CO, an oxygen atom was removed from CeO<sub>2</sub>, thus creating an oxygen vacancy, together with which single-atom Ru species participated in the activation of H<sub>2</sub>O. Currently, there are very few publications available on single-atom catalyzed methane oxidation in the fuel cell, and much more work needs to be done in this area.

#### Oxygenates Fuels

Compared with traditional gasoline fuel, oxygenates have lower toxicity, reduced CO<sub>2</sub> emissions, higher octane rating, and are more environmentally friendly and sustainable.<sup>55,56</sup> For example, the blending of 20% ethanol (one of the most common oxygenated fuels) in gasoline decreased the emission of CO, hydrocarbons, and NO<sub>x</sub> by 60%, 40%, and 20%, respectively.<sup>57</sup> It was also reported that every 10% addition of ethanol to gasoline could increase the octane number by 5 units.<sup>58</sup> According to the Renewable Fuels Association (RFA), the world ethanol production increased more than 100% from 13,123 million gallons in 2007 to 27,050 million gallons in 2017.

#### Biomass to Oxygenates Fuels

Currently, ethanol is mostly produced via fermentation of sugars derived glucose. The production of ethanol from lignocellulosic biomass is receiving major research

attention due to its easy availability, low cost, and minimal competition with food production.<sup>59</sup> Zhang and co-workers proposed a two-step transformations of lignocellulose to ethanol<sup>60</sup>: lignocellulose was firstly converted to methyl glycolate (MG), which then underwent hydrogenation to form ethanol on copper-based catalysts. To further improve the efficiency of the second step, a single-atom Pt@Cu alloy catalyst was employed. The single-atom Pt species improved Cu dispersion, promoted H<sub>2</sub> activation, and minimized C–C bond cleavage, thus enhancing the activity and selectivity of ethanol. Li and co-workers developed a single-atom Ru/C<sub>3</sub>N<sub>4</sub> catalyst, which showed temperature-dependent selectivity in the conversion of biomass-derived vanillin—a typical lignin model compound as a precursor for fuel additives.<sup>61</sup> The selective hydrodeoxygenation of vanillin to 2-methoxy-p-cresol is a widely studied model reaction for the much more complicated real biomass deoxygenation to fuel additives. Removal of oxygen is a critical issue for biomass upgrading, as the high oxygen content is the cause for low energy density, instability, corrosiveness, and high viscosity. Lower reaction temperature facilitated the hydrogenation of vanillin to form vanillyl alcohol, while higher temperature promoted the production of 2-methoxy-p-cresol via hydrodeoxygenation.

#### Methane to Oxygenates Fuels

The direct conversion of methane to oxygenated products using H<sub>2</sub>O<sub>2</sub> as an oxidant in the aqueous phase was performed on SACs. Tao and co-workers designed a single-atom Pd catalyst with 2.0% CuO on ZSM-5, which showed a TOF of 2.78 s<sup>-1</sup> with 86% selectivity toward methanol at 95°C.<sup>62</sup> Lee and co-workers reported five times recycling of single-atom Rh/ZrO<sub>2</sub> catalyst in the oxidation of methane to methanol by H<sub>2</sub>O<sub>2</sub> at 70°C without significant deactivation.<sup>50</sup> The graphene-confined single iron atoms were even active under ambient temperature for the direct conversion of methane to oxygenated fuels following a radical pathway.<sup>63</sup> Among various transition metals evaluated, only single-atom Fe was active due to the unique O–FeN<sub>4</sub>–O structure (Figure 4A). To understand the origin of activity, the methane activation rate as a function of formation energy (G<sub>f</sub>) of O–M<sub>N</sub><sub>4</sub>–O (M = Cr, Mn, Co, Ni, Cu) was determined (Figure 4B). Compared with other O–M<sub>N</sub><sub>4</sub>–O species, O–FeN<sub>4</sub>–O has a moderate free energy of formation (G<sub>f</sub>) and shows the best ability to compromise all the energy barriers, and thus exhibited the best performance for methane activation. Methane was also converted to methanol and other oxygenates using molecular O<sub>2</sub>, despite of the lower activity. In 2017, Flytzani-Stephanopoulos and co-workers reported that single Rh atoms dispersed on TiO<sub>2</sub> and ZSM-5 showed high performance in catalyzing the formation of acetic acid and methanol from methane using O<sub>2</sub> and CO under mild conditions.<sup>64</sup> After 3 h of reaction at 150°C, 21,295 micromoles of acetic acid and 230 micromoles of methanol per gram of catalysts were produced on Rh/ZSM-5 and Rh/TiO<sub>2</sub>, respectively. Tao and co-workers also reported similar results that single-atom Rh anchored on the wall of microporous ZSM-5 transferred methane to methanol, formic acid, and acetic acid through the coupling of methane, O<sub>2</sub>, and CO.<sup>65</sup>

#### CO<sub>2</sub> to Oxygenates Fuels

SACs catalyzed CO<sub>2</sub> hydrogenation into oxygenates such as methanol,<sup>66–69</sup> and formic acid<sup>36,70,71</sup> has been studied. The catalytic performance and reaction pathway of Pt single atoms Pt<sub>1</sub>@MIL and nanoparticle Pt<sub>n</sub>@MIL (MIL is a typical MOF which consists of μ<sub>3</sub>-oxo bridged Cr(III) trimers cross-linked by terephthalic acid) were compared during CO<sub>2</sub> hydrogenation to methanol.<sup>68</sup> The TOF and selectivity for methanol over Pt<sub>1</sub>@MIL was 5.6 times and 6.8 times higher, respectively, than that over Pt<sub>n</sub>@MIL. A significant amount of byproduct CO was produced over Pt<sub>n</sub>@MIL (Figure 4C). The reaction mechanism showed that COOH\* was the main

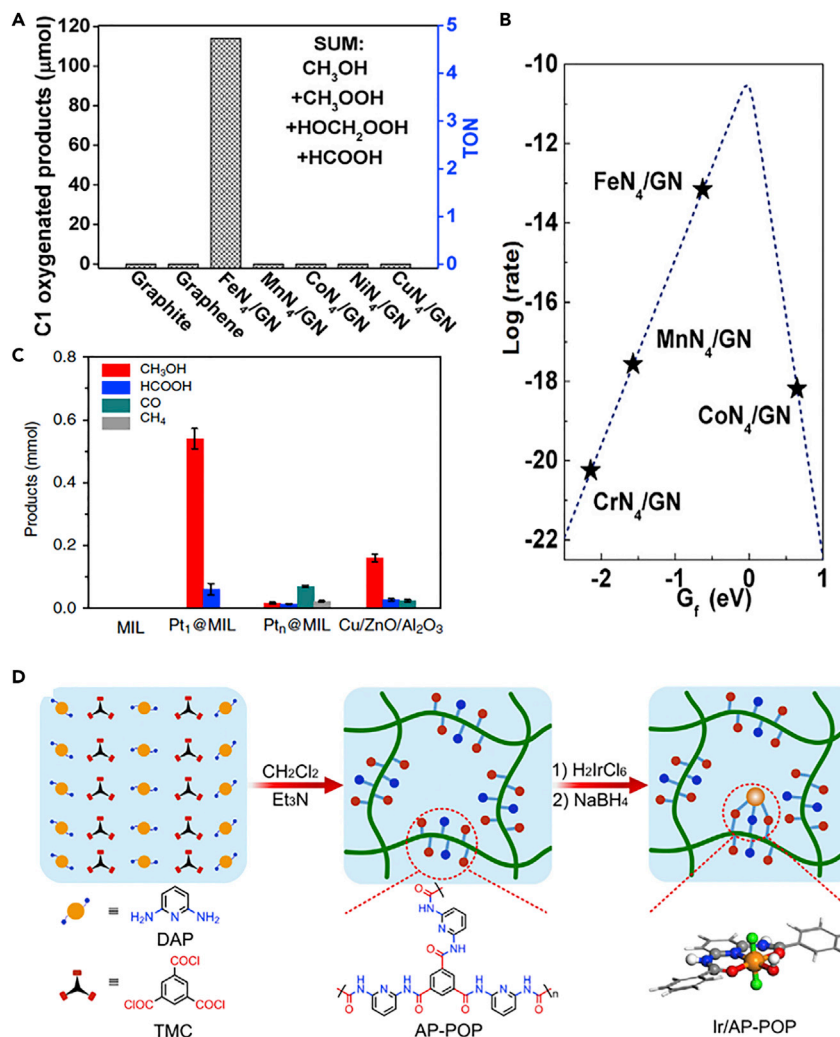


**Figure 4. SACs for the Transformation of Hydrocarbon Fuels**

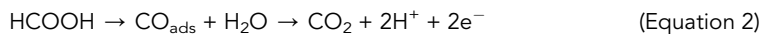
(A) Activity of graphite, graphene, Fe $\text{N}_4$ /GN, and other metal-N $_4$ /GN for methane oxidation.  
 (B) The methane activation rate [log(rate)] as a function of O–MN $_4$ –O active site formation energy(G $_f$ ).  
 (A) and (B) are reprinted from Bao et al.,<sup>63</sup> with permission. Copyright 2017, Cell Press.  
 (C) Catalytic performance of MIL-101, Pt $_1$ @MIL, Pt $_n$ @MIL, and commercial Cu/ZnO/Al $\text{}_2\text{O}_\text{3}$  for CO $_2$  hydrogenation. Reprinted from Zeng et al.,<sup>68</sup> with permission. Copyright 2019, Nature Publishing Group.  
 (D) A schematic illustration of the synthesis of Ir/AP-POP SAC. Reprinted from Zhang et al.,<sup>71</sup> with permission. Copyright 2019, Cell Press.

intermediate on the Pt $_n$ @MIL catalyst, while on Pt $_1$ @MIL the key intermediate was identified as HCOO\*. The distinct pathway over Pt $_1$ @MIL offered a lower energy barrier as well as the high selectivity for methanol production. The synergistic interaction between neighboring single metal atoms affects the reaction pathway as well as the activation energy in CO $_2$  hydrogenation.<sup>72</sup> Individual single-atom Pt preferred the hydrogenation of CO $_2$  into methanol, while both methanol and formic acid were formed over neighboring single Pt atoms. Zhang and co-workers designed a porous organic polymer (POP) with aminopyridine functionalities to anchor single-atom Ir for the conversion of CO $_2$  to formate (Figure 4D).<sup>71</sup> The formed polymeric framework (denoted as AP-POP) with electron-donating aminopyridine functional groups was used as support to disperse single-atom Ir via wet impregnation followed by

reduction. The fabricated single-atom Ir/AP-POP with an analogous structure to that of the homogeneous catalyst showed a turnover number (TON) of 25,135, representing one of the most active heterogeneous catalysts so far for formate synthesis from CO<sub>2</sub> hydrogenation.

#### *Electrocatalytic Oxidation of Formic Acid in Fuel Cells*

Formic acid electrocatalytic oxidation as the anodic reaction in the fuel cell has attracted intensive research activities. The formic acid oxidation reaction follows two pathways: in the direct pathway formic acid is converted to CO<sub>2</sub> ([Equation 1](#)); while in the indirect pathway CO is generated ([Equation 2](#)), leading to the deactivation of catalyst due to the strong affinity of CO to metal.<sup>73</sup>



In 2013, Lee and co-workers finely controlled the amount of Pt on Au nano-octahedra from single Pt atoms to Pt overayers, and the performance of different Pt species in formic acid electrocatalytic oxidation was compared.<sup>74</sup> The single-atom Pt showed a mass activity of 62.6 A/mg<sub>Pt</sub>, which was almost 10 times higher than that over Pt overayers. The single-atom Pt preferred the reaction pathway towards direct oxidation due to the absence of Pt nanoparticles and the bifunctional effects of Pt–Au sites. In 2018, a series of bimetallic PtAu nanoparticles with various Pt loading from 4% to 96% for formic acid oxidation were reported.<sup>75</sup> A similar conclusion was reached that single-atom Pt showed a higher resistance to CO poisoning, and exhibited orders of magnitude improvement in the oxidation of formic acid compared with Pt nanoparticles. DFT analysis indicated that the CO adsorption on single-atom Pt is weaker as a result of the electronic effects induced by the Pt–Au binding interaction as well as the discrete Pt active sites. To meet the requirements of practical application of single metal atoms catalysts in formic acid fuel cell, the loading of Pt was increased to 8 wt % while maintaining the atomic dispersion.<sup>76</sup> Single Pt atoms anchored on antimony-doped tin oxide (Pt<sub>1</sub>/ATO) maintained superior formic acid oxidation activity to the conventional Pt/C catalyst even after 1,800 cycles.

#### **H<sub>2</sub> Fuels**

H<sub>2</sub> is regarded as an ideal fuel for the future. The weight energy density of H<sub>2</sub> is 122 kJ/g, 2.75 times higher than that of hydrocarbon fuels.<sup>77</sup> According to the "Hydrogen Generation-Global Market Outlook (2017–2026)" report, the global H<sub>2</sub> production market is projected to reach \$207.48 billion by 2026 at an annual growth rate of 8.1% from the starting point of \$103.20 billion in 2017. It is predicted that 1 in 12 cars in South Korea, California, Japan, and Germany may be powered by hydrogen by 2030.<sup>78</sup> Hydrogen element is abundant in nature in the form of H<sub>2</sub>O, hydrocarbons, and biomass. However, a separate energy source such as electricity, light or heat is needed to extract H out of these sources in the form of H<sub>2</sub>. The main commercial H<sub>2</sub> production relies on steam reforming, oil reforming, coal gasification, and water electrolysis, accounting for 50%, 30%, 18%, and 2% respectively.<sup>79</sup> The overall challenge of using H<sub>2</sub> as fuel compounds comes from the ability to produce H<sub>2</sub> efficiently at low cost. Besides, compression energy for H<sub>2</sub> storage accounts for 10%–15% of the H<sub>2</sub> energy content. Single-atom metal catalysts make efficient use of the noble metal atoms and have found applications in H<sub>2</sub> production from methane or methanol reforming, water-gas shift reaction (WGSR), hydrogen evolution reaction (HER) and photocatalysis.

### H<sub>2</sub> Generation from Methane or Methanol Reforming

Steam methane reforming is the most commonly used method to produce H<sub>2</sub> in a large scale. One ton of H<sub>2</sub> production forms 9–12 tons of CO<sub>2</sub> in the process,<sup>80</sup> making it a significant contributor to CO<sub>2</sub> emission on earth.<sup>81</sup> McFarland and co-workers designed a stable molten Ni-Bi metal alloy catalyst, the active sites of which were atomically dispersed for the conversion of methane to H<sub>2</sub> and carbon without CO<sub>2</sub> and other byproduct formation at 1,065°C (Figures 5A–5D).<sup>82</sup> The previously used solid catalyst suffered severe deactivation due to carbon deposition, while the molten metal alloy showed stable performance in seven days of continuous operation. The formed carbon floated to the surface of the molten metal alloy where it was skimmed off easily. The H<sub>2</sub> production from methane at 1,100°C was also catalyzed by a single atom Fe@SiO<sub>2</sub> catalyst.<sup>48</sup> The concentration of H<sub>2</sub> in the effluent varied from 10.9% to 51.2% with the generation of value-added hydrocarbons (ethylene and aromatics) as by-products. The H<sub>2</sub> fuel was generated from methanol steam or aqueous-phase reforming. Ma and co-workers reported that atomically dispersed Pt on α-MoC exhibited superior low-temperature H<sub>2</sub> production activity as well as stability in aqueous phase methanol reforming, with an average activity of 18,046 mole of H<sub>2</sub> per moles of Pt per hour.<sup>83</sup> Due to the strong interaction between Pt and α-MoC, electron-deficient single Pt atoms were highly dispersed on the support, facilitating the adsorption and activation of methanol. Besides, the α-MoC promoted the dissociation of H<sub>2</sub>O to form abundant surface-bound hydroxyls, which benefited the reforming of active intermediates at the interfaces between α-MoC and single-atom Pt.

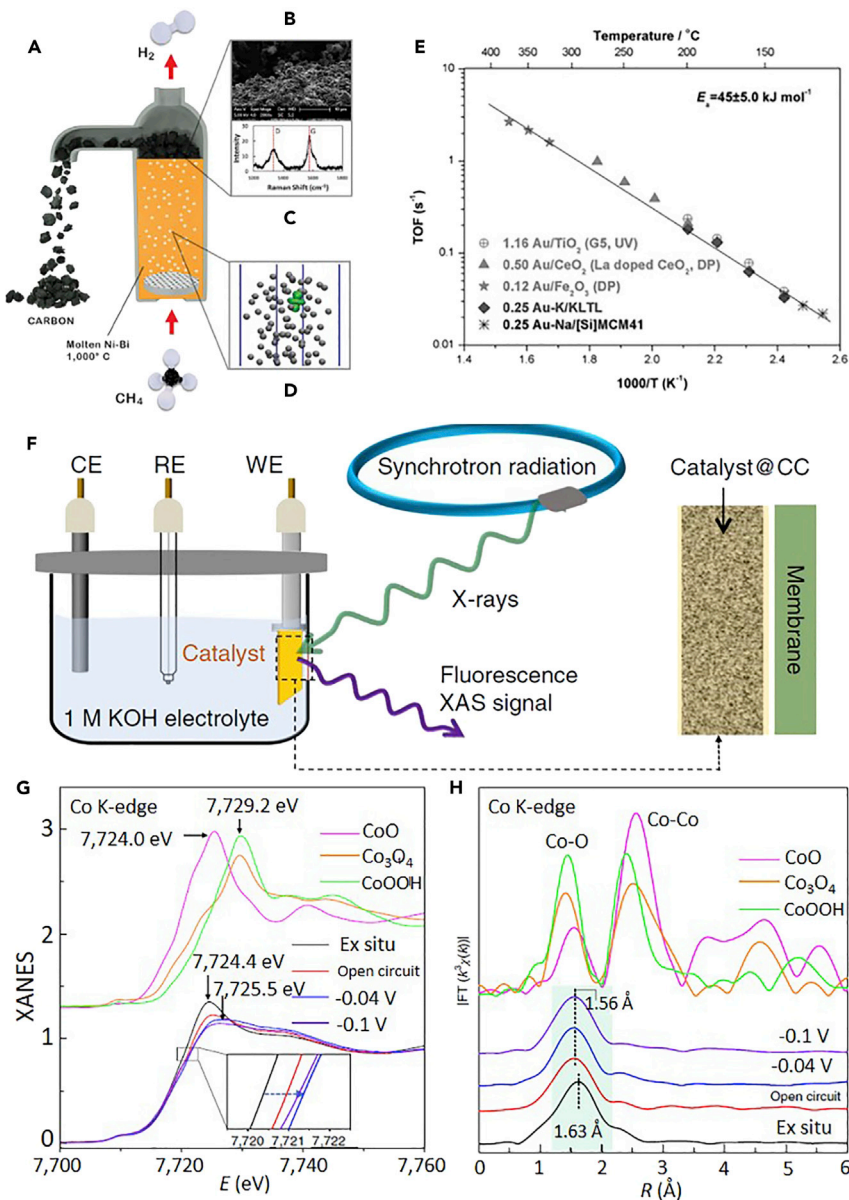
### H<sub>2</sub> Production from Water Gas Shift Reaction

Water-gas shift reaction (WGSR), an important industrial reaction to produce H<sub>2</sub> for energy application and to remove CO impurity in H<sub>2</sub> fuel cell, has been intensively studied on single-atom Au,<sup>8,84–86</sup> Pt,<sup>8,87–90</sup> Ir,<sup>91</sup> and Pd catalysts.<sup>92</sup> Flytzani-Stephanopoulos and co-workers proposed that positively charged Au and Pt SACs were active in WGS, while Au or Pt metal nanoparticles did not contribute significantly to the reaction as the removal of the particles by cyanide did not affect the activity.<sup>8,84</sup> Later, they reported that the addition of alkali ions (Na, K) helps to stabilize mononuclear Au or Pt atoms on zeolite KLTL and MCM-41 for low-temperature WGSR.<sup>85,90</sup> Besides, the activation energy of single-atom Au in WGS was independent of supports, regardless of inert supports such as KLTL and MCM-41 or reducible supports including TiO<sub>2</sub>, CeO<sub>2</sub>, and Fe<sub>2</sub>O<sub>3</sub> (Figure 5F). Zhang and co-workers also reported that single-atom Ir/FeO<sub>x</sub> catalyst showed more than 10 times activity of the Ir nanoparticles in WGSR.<sup>91</sup> The single-atom Ir improved the reducibility of FeO<sub>x</sub> and promoted the formation of oxygen vacancies, resulting in the excellent catalytic activity of single-atom Ir/FeO<sub>x</sub> catalyst.

### H<sub>2</sub> Production from HER

The hydrogen evolution reaction (HER), the cathodic half-reaction of water splitting, offers a reliable solution for the sustainable H<sub>2</sub> production. HER occurs through the reduction of protons (Equation 3) in acidic electrolytes or the reduction of water (Equation 4) in alkaline electrolytes.<sup>93</sup>



**Figure 5. SACs for the Production of  $\text{H}_2$  and  $\text{H}_2$  Fuel Cell**(A) Reactor for the conversion of  $\text{CH}_4$  to  $\text{H}_2$  and carbon in a molten-metal bubble column.

(B and C) SEM images (B) and Raman spectrum (C) of the formed carbon.

(D) Ab initio molecular dynamics simulation showing an orbital (green) of a Pt atom dissolved in molten Bi (gray) alloy. (A)–(D) are reprinted from McFarland et al.,<sup>82</sup> with permission. Copyright 2017, American Association for the Advancement of Science.(E) TOF plot for the WGS reaction over samples with atomically dispersed gold. Reprinted from Flytzani-Stephanopoulos et al.,<sup>85</sup> with permission. Copyright 2014, American Association for the Advancement of Science.(F) Schematic of the operando electrochemical cell set-up for identifying the active site of the  $\text{Co}_1/\text{PCN}$  electrocatalyst. CE, counterelectrode; WE, working electrode; RE, reference electrode.(G) Operando XANES spectra recorded at the Co K-edge of  $\text{Co}_1/\text{PCN}$ , at different applied voltages from the open-circuit condition to  $-0.1 \text{ V}$  during electrocatalytic HER, and the XANES data of the reference standards of  $\text{CoO}$ ,  $\text{Co}_3\text{O}_4$ , and  $\text{CoOOH}$ . Inset, Magnified pre-edge XANES region.(F)–(G) are reprinted from Wei et al.,<sup>117</sup> with permission. Copyright 2019, Nature Publishing Group.(H) Corresponding  $k^3$ -weighted Fourier transform (FT) spectra. The shaded region highlights the variations in the peak position and intensity.

Under standard temperature and pressure conditions, the enthalpy change for the formation of H<sub>2</sub> is 286 kJ/mol, which corresponds to a voltage of 1.23 V for the reversible electrolysis cell.<sup>94</sup> Under ideal conditions, an external potential of 1.23 V should be sufficient to drive the HER reaction. However, applying an overpotential is required to overcome the activation barriers and drive the electrochemical reaction. Efficient catalysts, mostly based on noble metals, can lower the overpotential.<sup>95,96</sup> To maximize the noble metal utilization efficiency, lower the catalyst cost, and improve the activity, selectivity as well as stability, the HER reaction has been carried out on single-atom noble metals,<sup>97</sup> such as Pt,<sup>98–100</sup> Pd,<sup>101</sup> Ru.<sup>102,103</sup> Besides, the HER reaction is also effectively promoted by non-noble metal SACs including Co<sup>104</sup> and Ni.<sup>105,106</sup>

Among the noble metal SACs in H<sub>2</sub> production from HER, single Pt atoms are the most widely studied. Single Pt atoms dispersed on nitrogen-doped graphene nanosheets (NGNs) by atomic layer deposition (ALD) technique exhibited as much as 37 times higher activity than the commercial Pt/C in HER, due to the partially unoccupied 5d states of single Pt atoms.<sup>107</sup> Wu and co-workers designed an ultra-low temperature ( $-60^{\circ}\text{C}$ ) ultraviolet photochemical method to prepare single-atom Pt and suppress the nucleation process of Pt atoms.<sup>108</sup> The prepared single-atom Pt catalyst exhibited lower overpotential (55 mV at 100 mA cm<sup>-2</sup>) and excellent stability in 5,000 cyclic voltammetry cycles. To understand the relationship between the coordination environment of single metal atoms and their catalytic performance, single-atom Pt catalysts with tunable coordination environment were dispersed on graphdiyne (GDY).<sup>109</sup> The four-coordinated Pt species (Pt-GDY1) were 3.3 times more active than five-coordinated Pt species (Pt-GDY2) in HER, due to the higher total unoccupied density of states of Pt 5d orbital and near to zero hydrogen adsorption Gibbs free energy on Pt-GDY2. Sun and co-workers reported that the electronic structure of single Pt atoms was modified by the coordination of nitrogen in aniline, showing superior HER performance and stability.<sup>110</sup> CO is often regarded as a poison ligand for Pt in heterogeneous catalysis, but Hyuck Choi and co-workers observed an unexpected improvement effect of CO on the performance of single-atom Pt in HER reaction.<sup>111</sup> The CO-ligation on the single-atom Pt promoted the dissociation of water to form H<sub>ads</sub> on Pt, thus enhancing the HER performance. Single Pt atoms were also used as co-catalysts to improve the HER performance. Two dimensional (2D) MoS<sub>2</sub>, as a potential alternative to Pt, has been studied in HER reaction. However, the performance of 2D-MoS<sub>2</sub> needs to be improved as only the edge sites of the 2D-MoS<sub>2</sub> contribute to the reaction while most sites at in-plane positions are inactive. Bao and co-workers doped single Pt atoms into the 2D MoS<sub>2</sub> via the substitution of Mo sites to trigger the HER activity of MoS<sub>2</sub>.<sup>112</sup> The doped single-atom Pt tuned the H atoms adsorption behavior on the neighboring S atoms, leading to a significant improvement of HER activity on MoS<sub>2</sub>.

Although noble metal SACs have shown excellent performance in H<sub>2</sub> production from HER, it is not undesirable to replace noble metals with non-noble metals to make H<sub>2</sub> a competitive energy carrier. The single Ni atoms dispersed on defective graphene showed a TOF of 0.3 s<sup>-1</sup>.<sup>113</sup> Although this value is almost one order of magnitude lower than that of the commercial Pt/C (2.30 s<sup>-1</sup>) at 50 mV overpotential,<sup>114</sup> platinum is four orders of magnitude more expensive than nickel.<sup>115</sup> The defective graphene offered a high density of anchoring sites through the efficient electron transfer between single-atom Ni and the 2 $\pi$  antibonding state of the adjacent carbon atoms.<sup>113</sup> Chen and co-workers dispersed single Ni atoms on nanoporous graphene for HER.<sup>116</sup> The unique sp-d orbital charge transfer between single atom Ni and the neighboring carbon atom resulted in a low overpotential around

50 mV. The dynamic structure of single-atom Co under alkaline HER condition was studied using operando X-ray absorption spectroscopy (Figure 5G).<sup>117</sup> The adsorption edge of the single-atom Co under open-circuit conditions was shifted towards higher energy side in comparison to *ex situ* samples; besides, a further shift was observed when the potentials of −0.04 and −0.1 V were applied (Figure 5H), indicating the oxidation state change of single-atom Co under working conditions. The operando EXAFS of single-atom Co showed different oscillation frequencies compared with the *ex situ* sample, and the intensity of Co–O/N peaks also changed when potentials were applied, suggesting a structural change of the single-atom Co under working conditions.

#### The Photocatalytic H<sub>2</sub> Production

The photocatalytic H<sub>2</sub> production under light irradiation is considered as a type of artificial photosynthesis.<sup>118</sup> Generally, the photocatalytic H<sub>2</sub> production involved the adsorption of light to generate electron-hole pairs, followed by charge separation and surface reaction. The overall photocatalytic performance is determined by both the thermodynamics and kinetics of the above steps.<sup>119</sup> Photocatalysts usually suffer from lower efficiency and selectivity towards H<sub>2</sub> evolution under solar energy due to the high probability of charge-hole recombination events. The utilization of single metal atoms, as a new form of co-catalyst, can suppress electron-hole recombination, thus increasing the H<sub>2</sub> photocatalytic production efficiency.<sup>120–123</sup> It was reported that single-atom Pt dispersed on C<sub>3</sub>N<sub>4</sub> dramatically enhanced the photocatalytic H<sub>2</sub> formation.<sup>124,125</sup> Ultrafast transient absorption spectroscopy indicated that the change of the intrinsic surface trap states in the support induced by the single Pt atoms contributed to the performance enhancement.<sup>125</sup> Due to the improved hydrogen binding energy, single-atom Pt confined into the metal-organic framework (MOF) exhibited a TOF 30 times greater than Pt nanoparticles.<sup>126</sup> Single-atom Pd/g-CN was reported to show a TOF of 417 h<sup>−1</sup>, which was much better than that of benchmark Pt/g-CN (76 h<sup>−1</sup>) for photocatalytic H<sub>2</sub> evolution reaction.<sup>101</sup> Hyeon and co-workers reported the design of highly active hollow TiO<sub>2</sub> photocatalyst with single-atom Cu anchored in the Ti vacancies.<sup>127</sup> The oxidation state change of single-atom Cu induced by the atomic localization of photogenerated electrons promoted the activation of neighboring TiO<sub>2</sub>, and improved the H<sub>2</sub> production performance dramatically.

#### H<sub>2</sub> Fuel Cell

H<sub>2</sub> fuel cells convert H<sub>2</sub> and O<sub>2</sub> to electricity with H<sub>2</sub>O and heat as the by-products. In comparison to other energy converters such as internal combustion engines and power plants, H<sub>2</sub> fuel cells are free of emissions besides H<sub>2</sub>O. Even if H<sub>2</sub> is produced by existing technology from non-renewable natural gas, the overall pollutant emission will be decreased by 30% for cars and trucks driven by H<sub>2</sub> in comparison to gasoline-powered counterparts.<sup>128</sup> Development of cost-effective and high-performance catalysts for the electrocatalytic oxygen reduction reaction (ORR) is key to realizing the large-scale application of H<sub>2</sub> fuel cells. The ORR occurring at the cathode of electrochemical energy devices proceeds via either a two-electron (2e<sup>−</sup>) or four-electron (4e<sup>−</sup>) pathway. The four-electron pathway that reduces oxygen directly into the water is highly preferred for batteries because of the high energy-conversion efficiency. The catalysts are the “heart” of the H<sub>2</sub> fuel cells, and noble metals, particularly Pt are the essential elements for the ORR catalysts. Increasing the utilization efficiency of noble metals by making them atomically dispersed, while not compromising the catalytic performance, have become a potential solution.<sup>129–131</sup> There is also considerable incentive to develop non-precious metal catalysts, such as Fe,<sup>132–134</sup> Co,<sup>135,136</sup> Mn,<sup>137,138</sup> Cu,<sup>139</sup> and Zn<sup>140</sup> to replace Pt-based ORR catalysts.<sup>141</sup>

The single Au atoms dispersed on TiC were fabricated for the ORR.<sup>114</sup> The TOF of single-atom Au/TiC ( $1.57\text{ s}^{-1}$ ) was almost 3 times higher than that of Au nanoparticles supported on TiC ( $0.54\text{ s}^{-1}$ ) during ORR in acidic solution at 0.2 V. A quasi-Pt-allotrope ORR catalyst consisting of hollow Pt<sub>3</sub>Co nanosphere as the core and N-doped carbon with single-atom Pt as the shell exhibited stable 4e<sup>-</sup> ORR over 10,000 cycles.<sup>142</sup> Single Ru atoms dispersed on N-doped graphene by forming Ru-N<sub>4</sub> moieties offered better resistance toward methanol, and CO poisoning than commercial Pt/C catalyst.<sup>143</sup>

Among the earth-abundant transition metal SACs, metal-nitrogen-carbon (M = Fe or Co) based catalysts have been regarded as one of the most promising candidates in ORR.<sup>136,144–147</sup> Li and co-workers reported single-atom Co catalysts, in which cobalt atoms were anchored in hierarchically porous N-doped carbon<sup>148</sup> and hollow N-doped carbon spheres.<sup>149</sup> A half-wave potential of 0.892 V—53 mV more positive than that of commercial Pt/C—was obtained on the designed single Co atoms. The promotional effect was attributed to the synergistic contribution from both isolated Co atoms and the unique 3D hierarchical porous structure of the carbon support.<sup>148</sup> Lin and co-workers compared the ORR performance of hierarchically porous Co–N–C and Fe–N–C SACs.<sup>150</sup> The Fe–N–C offered a half-wave potential of 0.972 V, which was 49 mV higher than that on Co–N–C, as the single-atom Fe–N–C promoted the release of OH\* intermediate, thus improving the ORR performance.

Fe-based catalysts have attracted great interest for ORR. Single-atom Fe species were anchored on graphene hollow nanospheres using SiO<sub>2</sub> as the template and Fe phthalocyanine as the precursor.<sup>151</sup> The rigid planar macrocycle structure of Fe precursor and the strong  $\pi$ – $\pi$  interaction between Fe precursor and graphene oxide were beneficial for the dispersion of Fe. The atomically dispersed Fe species showed excellent activity, stability for ORR and tolerance toward methanol, NO<sub>x</sub>, and SO<sub>2</sub> poisoning. The incorporation of S to single-atom Fe dispersed on nitrogen-doped carbon further improved the ORR activity due to the formation of thiophene-like structure (C–S–C) that decreased the electron localization of single-atom Fe.<sup>152</sup> The properties of the supports also have a great influence on the activity of the single-atom Fe catalysts.<sup>153</sup> Fe anchored on nitrogen-doped graphene with identical FeN<sub>4</sub>C<sub>12</sub> moieties were prepared by the pyrolysis in Ar or NH<sub>3</sub>. The ORR performance over NH<sub>3</sub>-pyrolyzed catalyst was much higher than that over Ar-pyrolyzed one, due to the formed basic N-groups in the NH<sub>3</sub> pyrolysis process. While some studies referred to the formation of Fe-pyrrolic-N structures as the origin of high performance of single-atom Fe catalyst confined in carbon supports,<sup>154</sup> another study suggested that the size of supports was also critical for the ORR activity.<sup>155</sup> In the range of 20 to 1000 nm, the best ORR activity was achieved at a particle size of 50 nm. Single-atom Fe bonded to graphdiyne through the formation of Fe–C also showed comparable activity as commercial Pt/C during ORR, in which single-atom Fe species promoted the reduction of oxygen directly into water while suppressing the formation of H<sub>2</sub>O<sub>2</sub>.<sup>156</sup>

### Batteries

Batteries have been regarded as promising candidates for sustainable energy storage and conversion because of the high energy density and low cost. ORR is a relevant process for both fuel cells and batteries. The rate-determining step of SACs in ORR is complicated and still under debate. While O<sub>2</sub> adsorption was identified as the rate-limiting step for single Zn atoms,<sup>140</sup> the reduction of adsorbed O<sub>2</sub> to OOH\*,<sup>143</sup> and the desorption of OH were proposed as the slowest step on single-atom Ru and

Pt, respectively.<sup>157</sup> The SACs showing exceptional performance in fuel-cell might also have the potential to be applied in batteries.<sup>158,159</sup> For example, single Fe atoms dispersed on the hollow carbon polyhedron containing N, P, and S as dopants were tested in H<sub>2</sub> fuel cell and Zn-air battery.<sup>159</sup> The designed catalysts delivered a superior current density of 400 mW/cm<sup>2</sup> at 0.40 eV in the H<sub>2</sub>-air-fuel test, comparable to that of commercial Pt/C catalyst. Moreover, the single-atom Pt, as the air cathode for the Zn-air battery, showed negligible voltage change after 500 cycle tests with 200,000 s; whereas a significant voltage decreased was observed on commercial Pt/C catalyst. In this section, we touch upon recent progress made on the utilization of SACs in batteries.

Single-atom Fe<sup>160–164</sup> and Co<sup>165</sup> have been integrated in Zn-air batteries in lab-scale and showed better stability than commercial Pt/C catalyst. Deng and co-workers reported that in comparison to nanoclusters and nanoparticles, single-atom Co showed the best activity, durability, and reversibility in Zn-air batteries.<sup>166</sup> Single-atom FeN<sub>4</sub> species dispersed on open-mesoporous N-doped-carbon nanofibers were used as the electrode in Mg-air batteries.<sup>167</sup> The prepared electrode offered high open-circuit voltage, long operating life, and excellent flexibility, which showed a potential application in wearable and bio-adaptable Mg-air batteries. Single-atom Co embedded on N-doped graphene was applied as a cathode in Zn-air batteries.<sup>168</sup> The formed Co–N–C moieties promoted the formation of Li<sub>2</sub>S in discharge process as well as the decomposition in the charge process.

### Ammonia

The development of the Haber-Bosch process—the catalytic hydrogenation of N<sub>2</sub> into ammonia—has enabled the strong population growth worldwide since the beginning of the twentieth century. For the first time, fertilizer could be produced synthetically on a large scale. For the last 100 years, the Haber-Bosch process has essentially not witnessed any major improvements and continues to constitute a major climate change driver consuming 1%–2% of global energy, predominantly because of the production of H<sub>2</sub> as the reducing agent. Mainly due to slow reaction kinetics, high temperatures (400–500°C) and pressure (150–250 bar) must be employed, and the reaction mixture must be passed through catalyst beds multiple times to achieve favorable conversions. As the equilibrium conversion is higher at low temperatures but the activation of the strong N–N triple bond is challenging, the development of efficient catalysts could significantly impact the ecological footprint of fertilizer production. SACs based on bimetallic catalyst structures have been proposed for this daunting task, and the development could further improve our knowledge on the active site structure during reaction conditions. Beyond thermal catalysis, more recent advances in photo- and electrocatalysis with SACs could prove promising as ambient pressure and temperatures are sufficient to achieve reasonable reaction rates for the fixation of nitrogen gas. Due to its high gravimetric hydrogen content of 17.8%, ammonia is often regarded as a potential hydrogen storage compound. Ammonia can be compressed under much lower pressure (10 bar) and temperature (−33°C) compared to hydrogen (−240°C). Furthermore, the concentration of N<sub>2</sub> in the air is 78.1% while that of CO<sub>2</sub> is 0.04% by volume rendering nitrogen-containing hydrogen storage compounds more straight-forward. Both the decomposition of ammonia into carbon-free hydrogen for hydrogen fuel cells and the use of direct ammonia fuel cells are envisioned.<sup>169,170</sup> Especially, energy storage on a small scale based on the conversion of stranded energy resources into a chemical storage compound may rely on the electrocatalytic production of ammonia.<sup>171</sup>

### The Electrocatalytic Nitrogen Reduction Reaction

Bimetallic alloys where one metal is atomically dispersed in a solid ‘solution’ of another metal are popular catalysts. On the very small side of this approach are bimetallic single-cluster catalysts like Rh<sub>1</sub>/Co<sub>3</sub> supported on cobalt oxide. Although this has been realized experimentally for the thermal reduction of NO to N<sub>2</sub> and N<sub>2</sub>O, it was recently proposed based on DFT calculations that among other single-cluster catalysts, Rh<sub>1</sub>/Co<sub>3</sub> would also be capable of reducing nitrogen into ammonia.<sup>172</sup> The capacity of the metal surrounding the atomically dispersed element to buffer charges and contribute to the catalytic reaction synergistically are believed to mainly contribute to the predicted catalytic performance (Figure 6A).

Different experimental studies have validated the use of SACs for the electrocatalytic nitrogen reduction reaction (NRR)—mostly based on Fe, Mo, and Ru. A nitrogen-doped carbon nanotube-supported Fe-based SAC synthesized by the pyrolysis of an iron-containing MOF reduced nitrogen to ammonia at −0.2 V versus RHE with Faradaic efficiencies of 9.28%, and a production rate of 34.83 μg h<sup>−1</sup> mg<sub>cat</sub><sup>−1</sup>. An iron species surrounded by 3 nitrogen atoms was proposed as the main active species and poisoning with thiocyanate salts showed that the nitrogen reduction activity was prohibited by the presence of Lewis bases. The mechanism was proposed to follow a distal pathway where dinitrogen binds in an end-on fashion on the Fe atoms, and the first ammonia production reaction occurs on the nitrogen atom more distant to Fe.<sup>173</sup> A Mo-based SAC supported on nitrogen-doped carbon material was synthesized in a similar pyrolysis procedure to the above-mentioned Fe SAC. Faradaic efficiencies of 14.6% ± 1.6% with an ammonia formation rate of 34.0 ± 3.6 μg h<sup>−1</sup> mg<sub>cat</sub><sup>−1</sup> were achieved at −0.3 V versus RHE in 0.1 mol L<sup>−1</sup> KOH solution. With around 10 wt % Mo loading, the catalyst does not exhibit a significant decrease in activity in 14 h and no formation of Mo clusters after the reaction was observed by HAADF-STEM.<sup>22</sup> Similar to the thermal catalytic reduction of nitrogen, Ru exhibits the best reaction rates achieved so far for the NRR using SACs. Using a MOF-pyrolysis procedure (Figure 6B), atomically dispersed Ru supported on nitrogen-doped carbon achieves Faradaic efficiencies of 29.6% at −0.2 V versus RHE with reaction rates of 120.9 μg h<sup>−1</sup> mg<sub>cat</sub><sup>−1</sup> in 0.05 mol L<sup>−1</sup> sulfuric acid. Again, the triple nitrogen-coordinated structure was proposed to be the active site.<sup>174</sup> The addition of ZrO<sub>2</sub> to Ru SACs supported on nitrogen-doped carbon was found to be sufficient to suppress the competing hydrogen evolution reaction, and ammonia Faradaic efficiencies of 21% were achieved at −0.21 V versus RHE with maximum ammonia formation rates of 3.67 mg h<sup>−1</sup> mg<sub>Ru</sub><sup>−1</sup>. A duration test over 60 h indicated high stability of the SAC under reaction conditions (Figure 6C). Plausibly, the presence of nitrogen in the carbon material and the addition of ZrO<sub>2</sub> are essential to not only enhance the stability and activity for electrochemical reactions but also improve the Faradaic efficiencies for ammonia production.<sup>175</sup>

Due to the importance of alternative ways to convert nitrogen gas into ammonia and the scarcity of experimentally reported catalysts, many DFT-based studies have been conducted to guide the rational catalyst design and screening. Similar to the best experimental systems, isolated Ru atoms supported on different nanoporous carbon materials have been predicted to be stable and active for the NRR, although the competing HER increases the necessary overpotential.<sup>176</sup> A systematic study of different transition metals on nitrogen-doped carbon employing three defined properties including stability, the competitive adsorption of dinitrogen against dihydrogen molecules, and the competition of the first dinitrogen protonation against hydrogen adsorption on metal sites. Based on this analysis, Co- and Cr-containing SACs are predicted to yield the highest activity and selectivity for ammonia

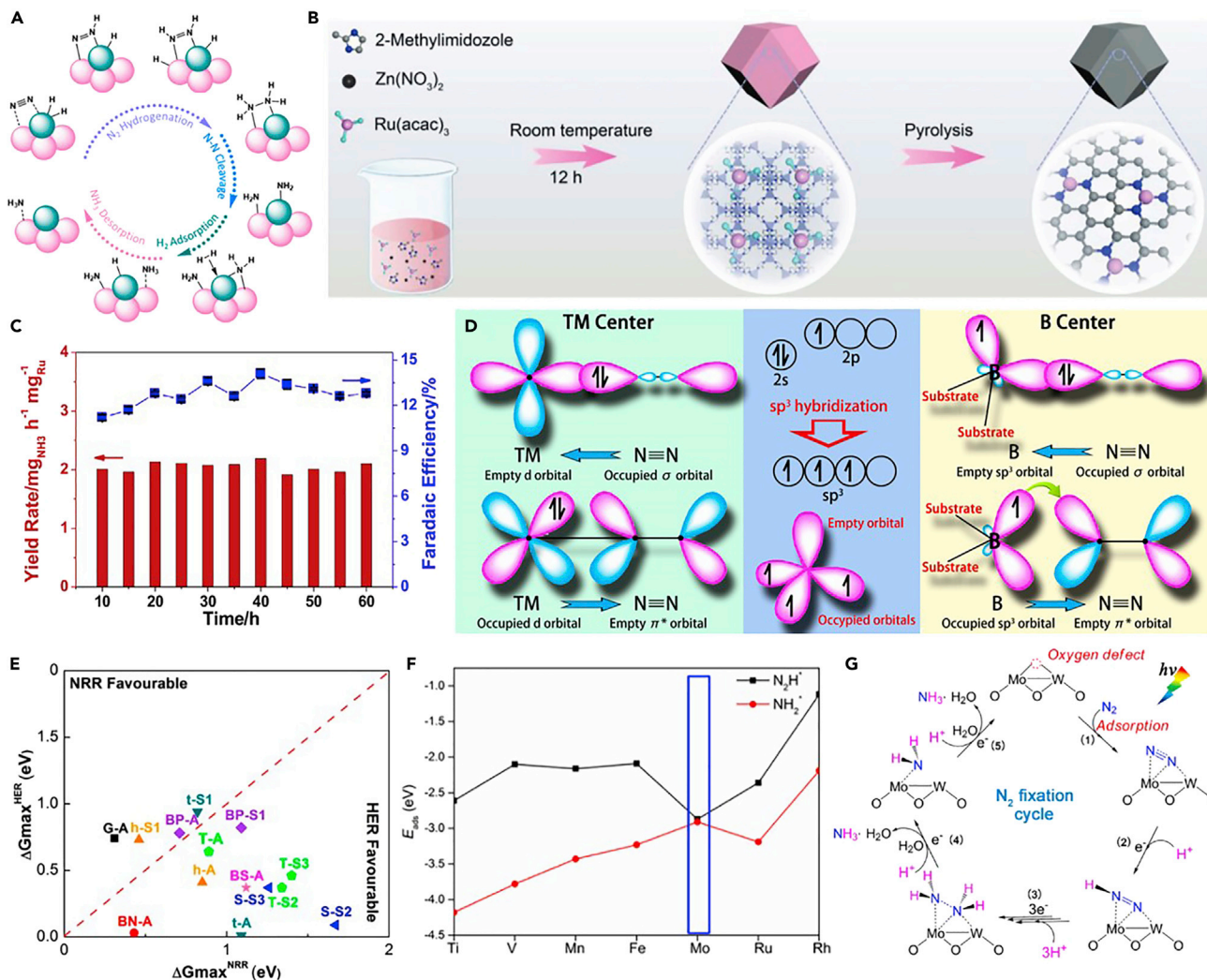


**Figure 6. Experimental Performance and DFT-Based Design Principles for Single-Atom Catalysed Nitrogen Reduction**

(A) Nitrogen hydrogenation reaction mechanism on Rh<sub>1</sub>CO<sub>3</sub> single cluster catalysts based on DFT calculations. Reprinted from Ma et al.,<sup>172</sup> with permission. Copyright 2018, American Chemical Society.

(B) MOF-pyrolysis-based synthesis procedure for Ru<sub>1</sub> supported on nitrogen-doped carbon. Reprinted from Geng et al.,<sup>174</sup> with permission. Copyright 2018, Wiley-VCH Verlag GmbH & Co. KGaA, Weinheim.

(C) Stability test for Ru<sub>1</sub> SAC on nitrogen-doped carbon for the NRR at -0.21 V at ~10°C. Reprinted from Tao et al.,<sup>175</sup> with permission. Copyright 2019, Elsevier.

(D) Schematic for the binding situation between dinitrogen and either transition metals or sp<sup>3</sup> hybridized boron atoms. Reprinted from Ling et al.,<sup>181</sup> with permission. Copyright 2018, American Chemical Society.

(E) Computational screening of 14 different catalyst combinations where the major descriptor for the NRR performance is plotted against the major descriptor for the HER activity. Reprinted from Liu et al.,<sup>244</sup> with permission. Copyright 2019, American Chemical Society.

(F) Adsorption energies of N<sub>2</sub>H and NH<sub>2</sub> species on different transition metal atoms supported on defective boron nitride nanosheets. Reprinted from Zhao et al.,<sup>178</sup> with permission. Copyright 2017, American Chemical Society.

(G) The proposed reaction mechanism for the photocatalytic nitrogen reduction on Mo-doped W<sub>18</sub>O<sub>49</sub>. Reprinted from Zhang et al.,<sup>180</sup> with permission. Copyright 2018, American Chemical Society.

production at low overpotentials.<sup>177</sup> Besides carbon-based materials, boron has been proposed as a powerful support and even active site for NRR. Upon binding of dinitrogen to sp<sup>3</sup>-hybridized boron atoms, the B-to-N π-back bonding populates N–N π\* orbitals and thus activates the notoriously strong N–N bond (Figure 6D). Depending on the support for isolated boron atoms, the NRR activity can be improved

while the HER activity can be suppressed (Figure 6E). Mo SACs supported on defective boron nitride with a boron monovacancy were calculated to surpass equivalent noble metal-based catalysts which were assigned to the unique ability of Mo to stabilize  $\text{N}_2\text{H}^*$  and destabilize  $\text{NH}_2^*$  species (Figure. 6F).<sup>178</sup> One of the challenges of utmost importance is the suppression of the HER under reaction conditions relevant for NRR which has been addressed recently by the computational comparison of 120 transition metal SACs supported on different nitrogen and carbon-containing scaffolds. The authors found that Ti and V have the strongest ability to activate dinitrogen as well as the lowest free energy barriers for the NRR while exhibiting little predicted HER activity.<sup>179</sup>

#### The Photocatalytic Nitrogen Reduction Reaction

The direct reduction of nitrogen into ammonia using sunlight as the sole energy source would be favorable but the development of efficient catalysts is a major challenge. Atomically dispersed copper on carbon nitride were shown to generate ammonia under the illumination of visible light (420 nm) with quantum efficiencies of around 1% and reaction rates of  $186 \mu\text{g h}^{-1} \text{ g}_{\text{cat}}^{-1}$  around 7 times higher than pure carbon nitride.<sup>65</sup> Doping isolated low-valent Mo atoms into  $\text{W}_{18}\text{O}_{49}$  nanowires was sufficient to enhance the catalytic activity by around 7 times compared to the undoped material and can achieve ammonia formation rates of  $195.5 \mu\text{g h}^{-1} \text{ g}_{\text{cat}}^{-1}$  with an apparent quantum efficiency of 0.028% under simulated AM 1.5 light irradiation. The interface between W and Mo was calculated to be the active site, and the reason for the enhanced catalytic performance (Figure 6G).<sup>180</sup> Similar to the NRR, boron atoms have been predicted to efficiently convert dinitrogen into ammonia on a semiconductor material such as carbon nitride. Besides the activation of dinitrogen molecules, boron atoms can enhance the visible light absorption of carbon nitride and thus are expected to improve the photocatalytic nitrogen reduction.<sup>181</sup>

#### Chemicals

Beyond the above-mentioned categories, the production of commodity and fine chemicals is closely connected to energy-consumption, providing access to agrochemicals, pharmaceuticals, polymers, fragrances, food additives, adhesives, lubricants, among others. According to the process intensification workshop held by U.S. Department of Energy in 2015, the overall US manufacturing sector in 2010 reached 19.24 quadrillion British thermal units (quads), where the chemical production processed consumed 1.15 quads.<sup>182</sup> Developing more efficient chemical process will reduce the energy consumption of the chemical sector and greenhouse gas emission. It becomes increasingly difficult to achieve full conversion while maintaining high selectivity for more complex chemicals, and therefore, laborious post-treatment becomes inevitable. Based on estimates by the Oak Ridge National Laboratory, separation processes account for around 15% of the total annual US energy consumption and for approximately 40%–50% of the total energy consumption in chemical processes.<sup>183,184</sup> More challenging separations such as in the pharmaceutical industries caused by very rigorous purity requirements and complex separation tasks such as the resolution of enantiomers would increase the energy consumption more significantly. Improving the selectivity of chemical reactions as well as replacing homogenous catalysts with suitable recyclable catalysts are thus imperative if the energy for separation is to be decreased. Besides offering the opportunity to conduct chemical reactions under milder and thus less energy-intensive conditions, SACs are also able to improve the reaction selectivity. For selective hydrogenation reactions where isomeric products or mixtures of alkynes, alkenes, and alkanes are particularly difficult to separate, SACs have proven to be excellent selective catalysts surpassing their nanoparticle counterparts. On the bridge between homogeneous

and heterogeneous catalysis, SACs have been shown to combine activity and selectivity for certain coupling and hydrofunctionalization reactions well beyond other heterogeneous catalysts while they are easily removed from the reaction solution by filtration. Besides, the catalysts can be used continuously when fixed bed reactor is applied.

#### *Hydrogenation Reactions*

Due to the absence of adjacent metal atoms, the activation of hydrogen and the subsequent hydrogenation reaction will occur much more selectively. One such example is the selective hydrogenation of acetylene – a major impurity hampering the ethylene polymerization reaction – to ethylene without promoting the complete hydrogenation to ethane. Similarly, the hydrogenation of butadiene, which is a strong poison for alkene polymerization catalysts, into the butene isomers requires the development of highly selective catalysts. Both positively charged SACs, as well as SAAs, have been used based on Pd,<sup>185–190</sup> Pt,<sup>191–194</sup> and Au<sup>9,10,195</sup> all of which showed selectivities for the semi-hydrogenation products far exceeding nanoparticle-based catalysts. Several other selective hydrogenation reactions have also been achieved, such as the chemoselective conversion of nitroaromatics to amines<sup>159,191,196,197</sup> and azo compounds<sup>198,199</sup> or the semi-hydrogenation of quinoline.<sup>200</sup> Compared to nanoparticle-catalysts, several SACs have been proven to be CO-tolerant hydrogenation catalysts probably due to the weak adsorption of CO on positively charged noble metals,<sup>201,202</sup> allowing the direct use of industrial-grade hydrogen gas as feedstock. Of note, the CO adsorption strength on single-atom Pt is still under debate. While some reports suggest CO adsorption on Pt<sub>1</sub> is much weaker than that on Pt nanoparticles,<sup>203</sup> other studies provide evidence for the strong adsorption of CO on single-atom Pt.<sup>204,205</sup>

Additionally, a Pt<sub>1</sub>/α-MoC catalyst offers high activity in the water-gas shift reaction so that water can be used as hydrogen source (Figure 7A).<sup>201</sup>

#### *Hydrofunctionalization Reactions*

SACs have been shown to show great promise for several hydrofunctionalizations reactions such as hydroformylation, hydrosilylation, and hydrochlorination reactions—all industrially relevant reactions where nanoparticle-based heterogeneous catalysts are inferior compared to homogeneous catalysts. Rh SACs supported on ZnO<sup>206</sup> or CoO<sup>207</sup> show high activity and simultaneously high selectivity of up to 95% toward a certain isomeric aldehyde in stark contrast to Rh clusters of higher nuclearity and most homogenous catalysts (Figure 7B).<sup>207</sup> The authors ascribe this enhanced reactivity to the dynamics of Rh atoms on the CoO support or the charge transfer from Zn to Rh on ZnO yielding almost metallic atomically dispersed Rh. Another application for atomically dispersed positively charged Pt atoms is the alkene hydrosilylation reaction, the arguably most important industrial application for homogenous Pt catalysts. Several Pt SACs and an SAA have been demonstrated for the hydrosilylation of different alkenes.<sup>208–211</sup> The high activity is normally attributed to either the high valence and thus the facile insertion of Pt into the C–H bond<sup>210</sup> or the charge transfer of Pd to Au in dilute Pd–Au alloys.<sup>211</sup> Recycling studies revealed that the SACs could be used up to 5 times without significant loss of activity with TONs of up to 10<sup>5</sup>. For the production of polyvinylchloride, the production of its monomer—vinylchloride—by the hydrochlorination reaction of acetylene is inevitable. The conventional heterogeneous industrial catalyst is based on toxic Hg, but recently single-site gold catalysts have been identified as a viable alternative. The reaction mechanism on carbon-supported Au has been experimentally proven to be based on an Au(I)–Au(III) redox cycle (Figure 7C).<sup>212,213</sup> In contrast, CeO<sub>2</sub>-supported Au catalysts follow an

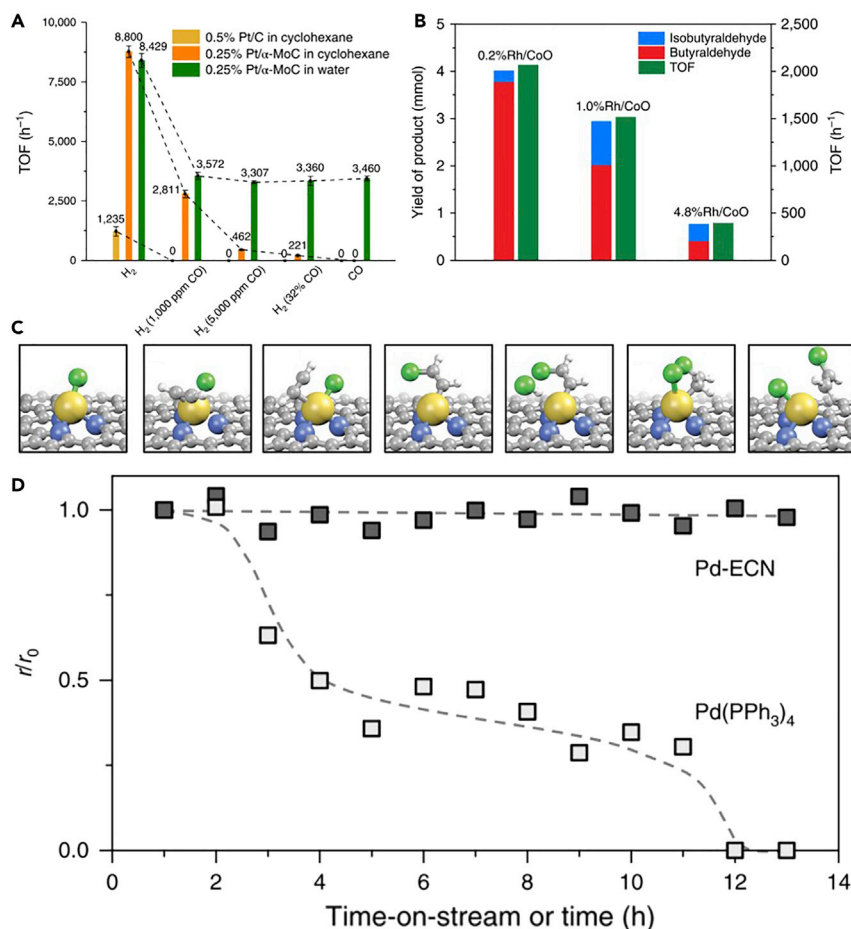


**Figure 7. SACs for Different Reactions to Produce Commodity and Fine Chemicals**

(A) Hydrogenation of nitrobenzene using a CO/H<sub>2</sub> gas mixture over different Pt-based SACs.

Reprinted from Lin et al.,<sup>201</sup> with permission. Copyright 2019, Nature Publishing Group.

(B) Hydroformylation of propylene at 100°C over different weight loadings of Rh supported on CoO.

(A) and (B) are reprinted from Wang et al.,<sup>207</sup> with permission. Copyright 2016, Nature Publishing Group.

(C) Calculated reaction pathway for the hydrochlorination reaction on Au single atoms on nitrogen-doped carbon. Reprinted from Kaiser et al.,<sup>213</sup> with permission. Copyright 2019, the Royal Society of Chemistry.

(D) Catalyst stability study for the continuous Suzuki coupling of bromobenzene with phenylboronic acid pinacol ester using a typical homogenous catalyst and a SAC. Reprinted from Chen et al.,<sup>219</sup> with permission. Copyright 2018, Nature Publishing Group.

Au(0)-Au(I) redox cycle because of electronic coupling with a Ce(IV)/Ce(III) cycle. The authors also show that catalytically inactive Au nanoparticles can decompose into isolated Au atoms when exposed to a C<sub>2</sub>H<sub>2</sub>/HCl mixture under reaction conditions.<sup>214</sup>

#### Coupling Reactions

Coupling reactions belong to the most important reactions in the synthesis of complex chemicals such as those in the pharmaceutical industries. Traditionally, heterogeneous nanoparticle catalysts are neither particularly active nor selective, and thus the sector mostly relies on the use of homogeneous catalysts which are inherently difficult and energetically expensive to recycle. Recently, different SACs have been shown to be active in the Ullmann,<sup>215</sup> Sonogashira,<sup>216,217</sup> Heck,<sup>216</sup> and

**Table 1. Reactions where SACs/SAAs Are Predominantly Reported to Be Superior or Inferior to NP Catalysts**

| Reactions where SACs/SAAs Are Predominantly Reported to Be Superior to NPs <sup>a</sup> | Reactions where SACs/SAAs Are Predominantly Reported to Be Inferior to NPs <sup>a</sup> | It Is Unclear or under Debate Whether SACs/SAAs Are Superior or NPs Are Superior |
|---|---|--|
| Hydroformylation  | Alcohol electrooxidation  | Methane activation to methanol   |
| Selective hydrogenation   |   |  |
| Alcohol oxidation   |   |  |
| Dehydrogenation of propane (SAAs)   |   |  |
| Water-gas shift   | Dehydrogenation of propane (SACs)   | N <sub>2</sub> hydrogenation   |
| Hydrogen evolution reaction   |   |  |
| Coupling reactions  |   |  |
| Oxygen reduction reaction   |   |  |

<sup>a</sup>Depending on the reaction, either the reaction rates or desired selectivity profiles are more relevant.

Suzuki<sup>216,218,219</sup> couplings. Besides the positive charge of noble metals in SACs resembling homogeneous metal complexes, the mobility of metal ions in supports such as carbon nitride was reported to be the reason for the catalytic activity sometimes surpassing homogeneous complexes. Recycling and flow reactor stability studies reveal that the SACs sustained coupling reactions over a long-time period in stark contrast to the stability of homogeneous complexes (Figure 7D).<sup>219</sup>

#### Dehydrogenation Reactions

Light olefins belong to the most crucial building blocks in the chemical industries. The recent exploitation of shale gas deposits spurred interest in the dehydrogenation reaction of light paraffins such as propane. Harsh reaction conditions resulting in catalyst stability issues as well as the formation of coke and other side products plague the development of suitable SACs. Pt SACs on CeO<sub>2</sub> are stable under propane dehydrogenation reaction conditions, but the selectivity towards propylene was negligible. This was assigned to the facile C–C bond cleavage on Pt<sub>1</sub> sites.<sup>220</sup> More recent calculations, however, indicated that SAAs with Pt diluted in more abundant metals such as Cu seem to combine both the excellent C–H activation capabilities of the noble metal and the low first dehydrogenation reaction barrier but prevent the further dehydrogenation of propylene to undesired side products. In fact, Pt/C SAAs are capable of breaking the scaling relationships between the propane dehydrogenation activity and selectivity commonly observed for single metal and alloy catalysts.<sup>221</sup> Similar turnover frequency (TOF) values of 0.72 s<sup>-1</sup> for Pt nanoparticles and 0.56 s<sup>-1</sup> for Pt/C SAAs at 520°C under otherwise identical reaction conditions were observed. Of note, the propylene selectivity was around 3.2 times higher for the SAA (90%) indicating a significantly better performance of SAA catalysts.<sup>221</sup> It was predicted based on DFT calculations that Pd/Cu SAAs would also exhibit favorable performance in the dehydrogenation of propane.<sup>222</sup>

#### Summary: The Good, the Bad, and the Unknowns

As shown in the sections above and summarized in Table 1, SACs have been reported to show superior catalytic activity to their nanoparticle counterparts in a wide range of catalytic applications, including hydroformylation to selective hydrogenation,<sup>185–194</sup> dehydrogenation,<sup>221,222</sup> water-gas shift reaction,<sup>8,84,91</sup> and hydrogen evolution reaction.<sup>98,107,108</sup> It is not unreasonable to propose, as a rule of thumb, that SACs may be superior to NPs in the reactions that are conventionally

more successful using metal complexes as catalysts. Likewise, the design of SACs should learn from the wisdom in homogeneous catalysis to fine-tune the frontier orbital geometry and energy of the active sites.

Meanwhile, SACs are not as active as nanoparticles in some other reactions. SACs might even be completely inactive in case that two or more neighboring metal atoms are required to activate a reactant. It is well-known that the electrooxidation of methanol in fuel cell dominantly involves three or four Pt atoms to accommodate the formed  $\text{CH}_x\text{O}$  intermediate.<sup>20</sup> The single-atom Pt dispersed on thiolated multiwalled carbon nanotubes (S-MWNTs) was almost inactive, while Pt nanoparticles were favorable for the methanol oxidation.<sup>223</sup> Similarly, Pt nanoclusters  $\text{Pt}_4$  and  $\text{Pt}_{10}$  anchored on indium tin oxide (ITO) showed excellent ethanol oxidation performance, while single-atom  $\text{Pt}_1/\text{ITO}$  was much less efficient.<sup>224</sup> Similarly, Pd ensembles rather than single-atom were proposed to be responsible for the ethanol oxidation reaction.<sup>225</sup> SACs could also be inferior to their nanoparticle counterparts in terms of reaction selectivity. For example, Pt SACs on  $\text{CeO}_2$ , when employed in propane dehydrogenation, exhibited negligible selectivity towards propylene due to facile C–C bond cleavage.<sup>220</sup>

Although SACs have received intensive research activities, deep understanding of the working mechanism of SACs is still under development. The debate remains regarding whether SACs are active or not in certain reactions, and if yes, whether they are more active than nanoparticle counterparts. Examples include CO oxidation, methane activation, and  $\text{N}_2$  hydrogenation. In the case of methane oxidation, Lee and co-workers argued that Rh single-atoms promoted the conversion of  $\text{CH}_4$  to methanol using  $\text{O}_2$  in the gas phase or  $\text{H}_2\text{O}_2$  in the aqueous solution,<sup>50</sup> while single Pd atoms were reported to be inactive for the same reaction.<sup>226</sup> For  $\text{N}_2$  hydrogenation, both experiment, and DFT simulation indicated that  $\text{N}_2$  dissociation on Ru(0001) was dominantly determined by the step sites,<sup>227</sup> whereas  $\text{N}_2$  reduction to ammonium was predicted to be feasible on single-atom Ru where step sites were not available.<sup>172,174,175</sup>

### Conclusions and Perspective

Single-atom catalysis emerges from the in-depth study of supported metal nanoparticle catalysts that already found wide industrial applications in oil refining, coal transformation, fertilizer production, and many more. Thanks to the technological advances in the spatial and temporal resolution of analytical tools, within merely a few years' time hundreds of reports generated in labs around the world authenticated the existence of the isolated single-atom species on various supports and their active participation in catalytic reactions. This does not only fundamentally change the way we view the structure and function of metal-based catalysts, but also provides grand opportunities for a more efficient usage of fossil resources, less energy-intensive processes for chemicals production, more effective energy storage and the novel transformations of alternative energy sources.

The development of efficient, selective, and stable catalysts with low cost is crucial for energy-related applications. Due to the maximized atom utilization efficiency and unparalleled electronic and geometric features, SACs have exhibited exciting technological, and fundamental significance in nearly every field of energy transformation and storage. In this review, the recent advances of SACs in the transformation of hydrocarbons, oxygenates,  $\text{H}_2$  fuel, batteries, ammonia, and fine chemicals have been summarized. Particular attention was paid to structure-performance relationship and the advantages of SACs in comparison to traditional nanoparticle or commercial catalysts in energy-related catalytic reactions. The prospect of using

SACs in energy application looks promising, and enormous advances have been achieved to date. However, future research should be devoted to the following aspects to foster further growth of the area, and potentially push the SACs for practical energy application.

#### *Challenges and Opportunities in the Synthesis of SACs*

Noble metal-based single atoms catalysts account for about two-thirds of published articles in the past five years.<sup>228</sup> Nevertheless, the non-precious SACs exhibiting comparable activity as noble-atom SACs are more attractive, given that performance and cost of catalysts are two important factors affecting the energy conversion. As discussed in the review, 3-d metal-based SACs exhibited comparable or even superior performances to noble-metal catalysts in several photocatalytic and electrocatalytic reactions. Future work should be directed to nitride or carbide supports combined with non-noble single metal atoms, which may offer unique electronic interactions with the metals generating improved performance.

Considering that many energy-related applications require harsh operation condition, the development of industrial-scale manufacturing methods that offer stable and high metal loading SACs at affordable cost is essential. Although several strategies have been reported along this line, these methods rely on strong anchoring sites on particular supports and therefore to a certain extent suffer from a lack of general applicability. Universal stabilization strategies for the synthesis of a wide range of SACs are pressingly needed. A possible approach is to learn from strategies to make stable colloidal nanoparticles,<sup>228</sup> such as electrostatic interaction and steric hindrance, which have been well studied and even quantitatively described in the past decades. On another note, despite that more than 80% of all the heterogeneous catalysts are fabricated by wet-chemical impregnation or precipitation,<sup>229</sup> it may not be ideal for every type of SACs synthesis since low loadings are necessary to keep the metals atomically dispersed. Very recently, a facile shockwave method was developed to synthesize thermally highly stable SACs.<sup>230</sup> Solid-state syntheses such as this one and other less conventional methods may find unique advantages in making SACs in the future.

#### *Grand Challenges in the Characterizations of SACs*

At present, the identification of single atoms is mainly achieved by the combined use of HAADF-STEM, CO-DRIFT-IR adsorption, and XAFS. While these techniques generate a clear picture of the structure of dominant metal species in a catalyst, none provides accurate electronic structure and coordination environment of the single metal atoms with spatial resolution under the working state. Therefore, the current understanding of the structures of active sites in complex heterogeneous SACs and their working mechanism in catalytic reactions are largely based on postulations derived from statistically averaged properties. A potential solution to the problem is the development of single-atom electron spectroscopy, which would enable structural identification of individual metal species under a microscope. This emerging technique has been successfully applied in the revealing localized electronic structure of single atoms,<sup>231</sup> but its usefulness to help understand the catalytic function of isolated metal atoms remains to be explored.

Another challenging and critical task in SACs is to develop a technique that does not only microscopically or spectroscopically image various metal species, but also differentiates which ones are active in catalysis and which ones are not. Often, various sized metal species coexist in a working heterogeneous catalyst. The contributions

of all these species in catalysis are hard to disentangle. Even for single-atom species, their structure and catalytic property are likely to be non-identical. Considering most catalytic reactions are associated with heat effect, active sites will induce a significant change of the local temperature. As such, we envisage sub-nanometer resolution thermometry combined with atomic resolution electron microscopy would offer a powerful tool to contrast metal species that are more active from the ones that are less active or completely inert. Recently, plasmons<sup>232</sup> and phonons<sup>233</sup> have been used to probe the temperature of nano-objects in the electron microscope. Leveraging on these advances, a thermometry-microscopy system for the above-mentioned application may become a reality.

#### *Remaining Challenges and Opportunities of SACs in the Context of Energy Conversion*

Although SACs have been intensively studied in various energy transformations, more research work should be devoted to expanding the application of SACs in even broader areas. We propose several reactions where SACs deserve further exploration: (1) Fischer-Tropsch synthesis. In industry, cobalt and iron nanoparticles are widely used. Metallic single-atom cobalt, iron or ruthenium alloys might offer unique selectivity in Fischer-Tropsch reaction; (2) Hydrocracking of heavy oil. Heavy oil hydrocracking is currently promoted by Pt nanoparticles supported on zeolites. A few single-atom Pt alloy catalysts have been successfully prepared in the literature.<sup>60,234</sup> It would be interesting to test the performance of these catalysts in hydrocracking despite their stability potentially representing an issue. (3) C–H activation. While methane activation has been realized by SACs, C–H activation of larger molecules such as benzene derivatives has rarely been reported. Considering that the Palladium complex is widely used in the C–H activation,<sup>235</sup> it deserves more effort to expand the application of SACs in C–H functionalization of more complicated substrates. (4) N≡N activation. Several DFT simulations for the hydrogenation of N<sub>2</sub> to NH<sub>3</sub> have been performed on SACs. It was predicted that SACs are promising for the conversion of N<sub>2</sub> to NH<sub>3</sub>. However, experimental validation of these reports is rare at the moment. Provided low temperature, pressure ammonia synthesis become viable, one could envisage decentralized facilities for NH<sub>3</sub> production and point distribution.

Along with the catalytic application of SACs getting increasingly broad, standardized operation protocols should be established for various reactions using SACs. When preparing this review, we realized that the performance of catalysts in most cases is measured under various conditions, making the comparison of catalytic behavior of SACs challenging. A good practice is surfacing. For instance, McCrory and co-workers developed a benchmarking protocol, using the potential increase after 2 h of galvanostatic polarization at 10 mA/cm<sup>2</sup> per geometric surface area to test the stability of OER catalysts.<sup>236,237</sup> More such efforts should be spent for the rational comparison of SACs in a broad range of energy-related applications.

#### *Opportunities for Computational and Machine-Learning Approaches in SACs*

The past few decades have witnessed a growing synergy between theoretical simulation and experimental investigations in catalysis. Traditionally, the DFT calculations were carried out within the concept of potential energy surface, in which a simplified model under idealized conditions (ultra-high vacuum and –273°C) was considered.<sup>238</sup> The fast development of hardware and software makes it possible to simulate the catalytic reactions under realistic conditions. A deeper understanding of the reaction mechanism and structure-performance relationship under

realistic conditions will benefit the rational design of single-atom catalysts for the specific energy transformation process.

The development of data science has enabled the big data strategies to discover the underlying correlations and making predictions. Machine learning for data analysis is spreading rapidly in catalysis,<sup>238</sup> and it is mainly focused on two aspects in heterogeneous catalysis: (1) the direct prediction of catalytic performance and (2) developing a model to estimate the reaction rate indirectly. Very recently, single-atom transition metals anchored on graphdiyne with outstanding electron transfer ability were identified using a deep-learning algorithm and big-data technique.<sup>239</sup> We anticipate growing employment of machine learning in guiding the design of particular SACs for energy transformation. Ideally, it is combined with fast synthetic platforms and high throughput performance screening techniques that have already been commercialized.

#### Bridging the Gap between Single-Atom Catalysts and Nanoparticle Catalysts

While hundreds of papers are available for SACs, only a handful of cases have been reported for dinuclear and multi-nuclear species without organic ligands as active sites.<sup>240–242</sup> There is a clear gap between SACs and well-studied nanoparticle catalysts. An atom-by-atom approach to synthesize active sites ranging from single-atoms to atomically precise metal clusters on the same support is highly desirable. In this regard, the concept of single-atom catalyst has been recently extended to single-cluster catalyst (SCC),<sup>172</sup> i.e., each catalyst bears only one type of  $M_x$  ( $x \geq 1$ ) species with a specific number of  $x$ . In this manner, the nuclearity effect in heterogeneous catalysis could be systematically studied, understood, and rationalized. The well-known B5 sites of Ru(0001) and the more recently proposed Fe<sub>3</sub> sites on 0-Al<sub>2</sub>O<sub>3</sub>(010)<sup>243</sup> for ammonia synthesis could both be considered as multi-nuclear metal sites. We expect research along this line will provide important new discovery in structure-activity correlations, which will ultimately benefit the identification of the best catalyst in each energy application.

#### ACKNOWLEDGMENTS

We thank the National University of Singapore Flagship Green Energy Program (R-279-000-553-646 and R-279-000-553-731) for financial support.

#### AUTHOR CONTRIBUTIONS

N.Y. and J.P.-R. conceived and supervised the preparation of the review. S.D., M.J.H., and N.Y. collected references and wrote the manuscript. N.Y. and J.P.-R. revised and finalized the manuscript. All authors approved the final version of the manuscript.

#### REFERENCES

1. Peters, A.W., Flank, W.H., and Davis, B.H. (2008). The history of petroleum cracking in the 20<sup>th</sup> century. In *Innovations in Industrial and Engineering Chemistry*, 1000 (American Chemical Society), pp. 103–187.
2. EIA International Energy Outlook 2016.
3. EIA International Energy Outlook 2017.
4. EIA International Energy Outlook 2018.
5. Maschmeyer, T., Rey, F., Sankar, G., and Thomas, J.M. (1995). Heterogeneous catalysts obtained by grafting metallocene complexes onto mesoporous silica. *Nature* 378, 159–162.
6. Abbet, S., Sanchez, A., Heiz, U., Schneider, W.-D., Ferrari, A.M., Pacchioni, G., and Rösch, N. (2000). Acetylene cyclotrimerization on supported size-selected Pd<sub>n</sub> clusters ( $1 \leq n \leq 30$ ): one atom is enough! *J. Am. Chem. Soc.* 122, 3453–3457.
7. Yamaguchi, K., Mori, K., Mizugaki, T., Ebitani, K., and Kaneda, K. (2000). Creation of a monomeric Ru species on the surface of hydroxyapatite as an efficient heterogeneous catalyst for aerobic alcohol oxidation. *J. Am. Chem. Soc.* 122, 7144–7145.
8. Fu, Q., Saltsburg, H., and Flytzani-Stephanopoulos, M. (2003). Active nonmetallic Au and Pt species on ceria-based water-gas shift catalysts. *Science* 301, 935–938.
9. Zhang, X., Shi, H., and Xu, B.Q. (2005). Catalysis by gold: isolated surface Au<sup>3+</sup> ions are active sites for selective hydrogenation of 1,3-butadiene over Au/ZrO<sub>2</sub> catalysts. *Angew. Chem. Int. Ed. Engl.* 44, 7132–7135.

10. Liu, Z.P., Wang, C.M., and Fan, K.N. (2006). Single gold atoms in heterogeneous catalysis: selective 1,3-butadiene hydrogenation over Au/ZrO<sub>2</sub>. *Angew. Chem. Int. Ed. Engl.* 45, 6865–6868.
11. Hackett, S.F.J., Brydson, R.M., Gass, M.H., Harvey, I., Newman, A.D., Wilson, K., and Lee, A.F. (2007). High-activity, single-site mesoporous Pd/Al<sub>2</sub>O<sub>3</sub> catalysts for selective aerobic oxidation of allylic alcohols. *Angew. Chem. Int. Ed. Engl.* 46, 8593–8596.
12. Wang, A., Li, J., and Zhang, T. (2018). Heterogeneous single-atom catalysis. *Nat. Rev. Chem.* 2, 65–81.
13. Qiao, B., Wang, A., Yang, X., Allard, L.F., Jiang, Z., Cui, Y., Liu, J., Li, J., and Zhang, T. (2011). Single-atom catalysis of CO oxidation using Pt1/FeOx. *Nat. Chem.* 3, 634–641.
14. Kunwar, D., Zhou, S., DelaRiva, A., Peterson, E.J., Xiong, H., Pereira-Hernández, X.I., Purdy, S.C., ter Veen, R., Brongersma, H.H., Miller, J.T., et al. (2019). Stabilizing high metal loadings of thermally stable platinum single atoms on an industrial catalyst support. *ACS Catal.* 9, 3978–3990.
15. Datye, A., and Wang, Y. (2018). Atom trapping: a novel approach to generate thermally stable and regenerable single-atom catalysts. *Natl. Sci. Rev.* 5, 630–632.
16. Chen, Y., Ji, S., Chen, C., Peng, Q., Wang, D., and Li, Y. (2018). Single-atom catalysts: synthetic strategies and electrochemical applications. *Joule* 2, 1242–1264.
17. Jiao, L., and Jiang, H.-L. (2019). Metal-organic-framework-based single-atom catalysts for energy applications. *Chem* 5, 786–804.
18. Peng, Y., Lu, B., and Chen, S. (2018). Carbon-supported single atom catalysts for electrochemical energy conversion and storage. *Adv. Mater.* 30, e1801995.
19. Wang, Y., Mao, J., Meng, X., Yu, L., Deng, D., and Bao, X. (2019). Catalysis with two-dimensional materials confining single atoms: concept, design, and applications. *Chem. Rev.* 119, 1806–1854.
20. Zhu, C., Fu, S., Shi, Q., Du, D., and Lin, Y. (2017). Single-atom electrocatalysts. *Angew. Chem. Int. Ed. Engl.* 56, 13944–13960.
21. Wang, B., Cai, H., and Shen, S. (2019). Single metal atom photocatalysis. *Small Methods* 3, 1800447.
22. Wang, Q., Zhang, D., Chen, Y., Fu, W.-F., and Lv, X.-J. (2019). Single-atom catalysts for photocatalytic reactions. *ACS Sustainable Chem. Eng.* 7, 6430–6443.
23. Liu, L., and Corma, A. (2018). Metal catalysts for heterogeneous catalysis: from single atoms to nanoclusters and nanoparticles. *Chem. Rev.* 118, 4981–5079.
24. Yang, X.F., Wang, A., Qiao, B., Li, J., Liu, J., and Zhang, T. (2013). Single-atom catalysts: a new frontier in heterogeneous catalysis. *Acc. Chem. Res.* 46, 1740–1748.
25. Schobert, H.H. (1990). *The Chemistry of Hydrocarbon Fuels*, First edition, p. 356.
26. Kunkes, E.L., Simonetti, D.A., West, R.M., Serrano-Ruiz, J.C., Gärtner, C.A., and Dumesic, J.A. (2008). Catalytic conversion of biomass to monofunctional hydrocarbons and targeted liquid-fuel classes. *Science* 322, 417–421.
27. Huber, G.W., Iborra, S., and Corma, A. (2006). Synthesis of transportation fuels from biomass: chemistry, catalysts, and engineering. *Chem. Rev.* 106, 4044–4098.
28. Liu, G., Robertson, A.W., Li, M.M., Kuo, W.C.H., Darby, M.T., Muñoz-Díez, M.H., Lin, Y.C., Suenaga, K., Stamatakis, M., Warner, J.H., et al. (2017). MoS<sub>2</sub> monolayer catalyst doped with isolated Co atoms for the hydrodeoxygenation reaction. *Nat. Chem.* 9, 810–816.
29. Duan, H., Dong, J., Gu, X., Peng, Y.K., Chen, W., Issariyakul, T., Myers, W.K., Li, M.J., Yi, N., Kilpatrick, A.F.R., et al. (2017). Hydrodeoxygenation of water-insoluble bio-oil to alkanes using a highly dispersed Pd-Mo catalyst. *Nat. Commun.* 8, 591.
30. Keith, D.W., Holmes, G., St. Angelo, D., and Heidel, K. (2018). A process for capturing CO<sub>2</sub> from the atmosphere. *Joule* 2, 1573–1594.
31. Zhang, C., Yang, S., Wu, J., Liu, M., Yazdi, S., Ren, M., Sha, J., Zhong, J., Nie, K., Jalilov, A.S., et al. (2018). Electrochemical CO<sub>2</sub> reduction with atomic iron-dispersed on nitrogen-doped graphene. *Adv. Energy Mater.* 8, 1703487.
32. Gu, J., Hsu, C.S., Bai, L., Chen, H.M., and Hu, X. (2019). Atomically dispersed Fe<sup>3+</sup> sites catalyze efficient CO<sub>2</sub> electroreduction to CO. *Science* 364, 1091–1094.
33. Matsuba, J.C., Yang, V.N., and Christopher, P. (2015). Isolated metal active site concentration and stability control catalytic CO<sub>2</sub> reduction selectivity. *J. Am. Chem. Soc.* 137, 3076–3084.
34. Yang, H.B., Hung, S.-F., Liu, S., Yuan, K., Miao, S., Zhang, L., Huang, X., Wang, H.-Y., Cai, W., Chen, R., et al. (2018). Atomically dispersed Ni(I) as the active site for electrochemical CO<sub>2</sub> reduction. *Nat. Energy* 3, 140–147.
35. Zhang, H., Wei, J., Dong, J., Liu, G., Shi, L., An, P., Zhao, G., Kong, J., Wang, X., Meng, X., et al. (2016). Efficient visible-light-driven Carbon dioxide reduction by a single-atom implanted metal-organic framework. *Angew. Chem. Int. Ed. Engl.* 55, 14310–14314.
36. Gao, G., Jiao, Y., Waclawik, E.R., and Du, A. (2016). Single atom (Pd/Pt) supported on graphitic carbon nitride as an efficient photocatalyst for visible-light reduction of Carbon dioxide. *J. Am. Chem. Soc.* 138, 6292–6297.
37. Cheng, M.-J., Clark, E.L., Pham, H.H., Bell, A.T., and Head-Gordon, M. (2016). Quantum mechanical screening of single-atom bimetallic alloys for the selective reduction of CO<sub>2</sub> to C<sub>1</sub> hydrocarbons. *ACS Catal.* 6, 7769–7777.
38. Abild-Pedersen, F., Greeley, J., Studt, F., Rossmeisl, J., Munter, T.R., Moses, P.G., Skúlasdóttir, E., Bligaard, T., and Nørskov, J.K. (2007). Scaling properties of adsorption energies for hydrogen-containing molecules on transition-metal surfaces. *Phys. Rev. Lett.* 99, 016105.
39. Back, S., and Jung, Y. (2017). TiC- and TiN-supported single-atom catalysts for dramatic improvements in CO<sub>2</sub> electrochemical reduction to CH<sub>4</sub>. *ACS Energy Lett.* 2, 969–975.
40. Wang, Y., Chen, Z., Han, P., Du, Y., Gu, Z., Xu, X., and Zheng, G. (2018). Single-atomic Cu with multiple oxygen vacancies on ceria for electrocatalytic CO<sub>2</sub> reduction to CH<sub>4</sub>. *ACS Catal.* 8, 7113–7119.
41. Kondratenko, E.V., Peppel, T., Seeburg, D., Kondratenko, V.A., Kalevaru, N., Martin, A., and Wohlrab, S. (2017). Methane conversion into different hydrocarbons or oxygenates: current status and future perspectives in catalyst development and reactor operation. *Catal. Sci. Technol.* 7, 366–381.
42. Chynoweth, D.P., Owens, J.M., and Legrand, R. (2001). Renewable methane from anaerobic digestion of biomass. *Renew. Energy* 22, 1–8.
43. McFarland, E. (2012). Chemistry. Unconventional chemistry for unconventional natural gas. *Science* 338, 340–342.
44. Lunsford, J.H. (2000). Catalytic conversion of methane to more useful chemicals and fuels: a challenge for the 21<sup>st</sup> century. *Catal. Today* 63, 165–174.
45. Nahreen, S., Prasertdam, S., Perez Beltran, S., Balbuena, P.B., Adhikari, S., and Gupta, R.B. (2016). Catalytic upgrading of methane to higher hydrocarbon in a nonoxidative chemical conversion. *Energy Fuels* 30, 2584–2593.
46. Sofranko, J.A., Leonard, J.J., and Jones, C.A. (1987). The oxidative conversion of methane to higher hydrocarbons. *J. Catal.* 103, 302–310.
47. Morejudo, S.H., Zanón, R., Escolástico, S., Yuste-Tirados, I., Malerød-Fjeld, H., Vestre, P.K., Coors, W.G., Martínez, A., Norby, T., Serra, J.M., et al. (2016). Direct conversion of methane to aromatics in a catalytic co-ionic membrane reactor. *Science* 353, 563–566.
48. Guo, X., Fang, G., Li, G., Ma, H., Fan, H., Yu, L., Ma, C., Wu, X., Deng, D., Wei, M., et al. (2014). Direct, nonoxidative conversion of methane to ethylene, aromatics, and hydrogen. *Science* 344, 616–619.
49. Xie, P., Pu, T., Nie, A., Hwang, S., Purdy, S.C., Yu, W., Su, D., Miller, J.T., and Wang, C. (2018). Nanoceria-supported single-atom platinum catalysts for direct methane conversion. *ACS Catal.* 8, 4044–4048.
50. Kwon, Y., Kim, T.Y., Kwon, G., Yi, J., and Lee, H. (2017). Selective activation of methane on single-atom catalyst of rhodium dispersed on zirconia for direct conversion. *J. Am. Chem. Soc.* 139, 17694–17699.
51. Murray, E.P., Tsai, T., and Barnett, S.A. (1999). A direct-methane fuel cell with ceria-based anode. *Nature* 400, 649–651.
52. Park, S., Vohs, J.M., and Gorte, R.J. (2000). Direct oxidation of hydrocarbons in a solid-oxide fuel cell. *Nature* 404, 265–267.

53. Shao, Z., and Haile, S.M. (2004). A high-performance cathode for the next generation of solid-oxide fuel cells. *Nature* 431, 170–173.
54. Chen, Y., deGlee, B., Tang, Y., Wang, Z., Zhao, B., Wei, Y., Zhang, L., Yoo, S., Pei, K., Kim, J.H., et al. (2018). A robust fuel cell operated on nearly dry methane at 500°C enabled by synergistic thermal catalysis and electrocatalysis. *Nat. Energy* 3, 1042–1050.
55. Rajasekar, E., Murugesan, A., Subramanian, R., and Nedunchezhan, N. (2010). Review of NO<sub>x</sub> reduction technologies in CI engines fuelled with oxygenated biomass fuels. *Renew. Sustain. Energy Rev.* 14, 2113–2121.
56. Awad, O.I., Mamat, R., Ibrahim, T.K., Hammid, A.T., Yusri, I.M., Hamidi, M.A., Humada, A.M., and Yusop, A.F. (2018). Overview of the oxygenated fuels in spark ignition engine: environmental and performance. *Renew. Sustain. Energy Rev.* 91, 394–408.
57. Liao, S.Y., Jiang, D.M., Cheng, Q., Huang, Z.H., and Wei, Q. (2005). Investigation of the cold-start combustion characteristics of ethanol-gasoline blends in a constant-volume chamber. *Energy Fuels* 19, 813–819.
58. Chen, R.-H., Chiang, L.-B., Chen, C.-N., and Lin, T.-H. (2011). Cold-start emissions of an SI engine using ethanol-gasoline blended fuel. *Appl. Therm. Eng.* 31, 1463–1467.
59. Isikgor, F.H., and Becer, C.R. (2015). Lignocellulosic biomass: a sustainable platform for the production of bio-based chemicals and polymers. *Polym. Chem.* 6, 4497–4559.
60. Yang, C., Miao, Z., Zhang, F., Li, L., Liu, Y., Wang, A., and Zhang, T. (2018). Hydrogenolysis of methyl glycolate to ethanol over a Pt–Cu/SiO<sub>2</sub> single-atom alloy catalyst: a further step from cellulose to ethanol. *Green Chem.* 20, 2142–2150.
61. Tian, S., Wang, Z., Gong, W., Chen, W., Feng, Q., Xu, Q., Chen, C., Chen, C., Peng, Q., Gu, L., et al. (2018). Temperature-controlled selectivity of hydrogenation and hydrodeoxygenation in the conversion of biomass molecule by the Ru<sub>1</sub>/mpg-C<sub>3</sub>N<sub>4</sub> catalyst. *J. Am. Chem. Soc.* 140, 11161–11164.
62. Huang, W., Zhang, S., Tang, Y., Li, Y., Nguyen, L., Li, Y., Shan, J., Xiao, D., Gagne, R., Frenkel, A.I., et al. (2016). Low-temperature transformation of methane to methanol on Pd<sub>1</sub>O<sub>4</sub> single sites anchored on the internal surface of microporous silicate. *Angew. Chem. Int. Ed. Engl.* 55, 13441–13445.
63. Cui, X., Li, H., Wang, Y., Hu, Y., Hua, L., Li, H., Han, X., Liu, Q., Yang, F., He, L., et al. (2018). Room-temperature methane conversion by graphene-confined single iron atoms. *Chem. 4*, 1902–1910.
64. Shan, J., Li, M., Allard, L.F., Lee, S., and Flytzani-Stephanopoulos, M. (2017). Mild oxidation of methane to methanol or acetic acid on supported isolated rhodium catalysts. *Nature* 551, 605–608.
65. Tang, Y., Li, Y., Fung, V., Jiang, D.E., Huang, W., Zhang, S., Iwasawa, Y., Sakata, T., Nguyen, L., Zhang, X., et al. (2018). Single rhodium atoms anchored in micropores for efficient transformation of methane under mild conditions. *Nat. Commun.* 9, 1231.
66. Back, S., Lim, J., Kim, N.Y., Kim, Y.H., and Jung, Y. (2017). Single-atom catalysts for CO<sub>2</sub> electroreduction with significant activity and selectivity improvements. *Chem. Sci.* 8, 1090–1096.
67. Ling, C., Li, Q., Du, A., and Wang, J. (2018). Computation-aided design of single-atom catalysts for one-pot CO<sub>2</sub> capture, activation, and conversion. *ACS Appl. Mater. Interfaces* 10, 36866–36872.
68. Chen, Y., Li, H., Zhao, W., Zhang, W., Li, J., Li, W., Zheng, X., Yan, W., Zhang, W., Zhu, J., et al. (2019). Optimizing reaction paths for methanol synthesis from CO<sub>2</sub> hydrogenation via metal-ligand cooperativity. *Nat. Commun.* 10, 1885.
69. Zhao, Z., and Lu, G. (2019). Cu-based single-atom catalysts boost electroreduction of CO<sub>2</sub> to CH<sub>3</sub>OH: first-principles predictions. *J. Phys. Chem. C* 123, 4380–4387.
70. Mori, K., Taga, T., and Yamashita, H. (2017). Isolated single-atomic Ru catalyst bound on a layered double hydroxide for hydrogenation of CO<sub>2</sub> to formic acid. *ACS Catal.* 7, 3147–3151.
71. Shao, X., Yang, X., Xu, J., Liu, S., Miao, S., Liu, X., Su, X., Duan, H., Huang, Y., and Zhang, T. (2019). Iridium single-atom catalyst performing a Quasi-homogeneous hydrogenation transformation of CO<sub>2</sub> to formate. *Chem* 5, 693–705.
72. Li, H., Wang, L., Dai, Y., Pu, Z., Lao, Z., Chen, Y., Wang, M., Zheng, X., Zhu, J., Zhang, W., et al. (2018). Synergistic interaction between neighbouring platinum monomers in CO<sub>2</sub> hydrogenation. *Nat. Nanotechnol.* 13, 411–417.
73. Yang, S., Kim, J., Tak, Y.J., Soon, A., and Lee, H. (2016). Single-atom catalyst of platinum supported on titanium nitride for selective electrochemical reactions. *Angew. Chem. Int. Ed. Engl.* 55, 2058–2062.
74. Yang, S., and Lee, H. (2013). Atomically dispersed platinum on gold nano-octahedra with high catalytic activity on formic acid oxidation. *ACS Catal.* 3, 437–443.
75. Duchesne, P.N., Li, Z.Y., Deming, C.P., Fung, V., Zhao, X., Yuan, J., Regier, T., Aldalbahi, A., Almarhoon, Z., Chen, S., et al. (2018). Golden single-atomic-site platinum electrocatalysts. *Nat. Mater.* 17, 1033–1039.
76. Kim, J., Roh, C.-W., Sahoo, S.K., Yang, S., Bae, J., Han, J.W., and Lee, H. (2018). Highly durable platinum single-atom alloy catalyst for electrochemical reactions. *Adv. Energy Mater.* 8, 1701476.
77. Singh, A., Sevda, S., Abu Reesh, I., Vanbroekhoven, K., Rathore, D., and Pant, D. (2015). Biohydrogen production from lignocellulosic biomass: technology and sustainability. *Energies* 8, 13062–13080.
78. Council, H. (2017) Hydrogen Scaling up A Sustainable Pathway for the Global Energy Transition.
79. Grand View Research. (2018). Hydrogen generation market analysis and segment forecast to 2025, 1–140.
80. Collodi, G., and Wheeler, F. (2010). Hydrogen production via steam reforming with CO<sub>2</sub> capture. *Chem. Eng. Trans.* 19, 37–42.
81. Wismann, S.T., Engbæk, J.S., Vendelbo, S.B., Bendixen, F.B., Eriksen, W.L., Aasberg-Petersen, K., Frandsen, C., Chorkendorff, I., and Mortensen, P.M. (2019). Electrified methane reforming: a compact approach to greener industrial hydrogen production. *Science* 364, 756–759.
82. Upham, D.C., Agarwal, V., Khechfe, A., Snodgrass, Z.R., Gordon, M.J., Metiu, H., and McFarland, E.W. (2017). Catalytic molten metals for the direct conversion of methane to hydrogen and separable carbon. *Science* 358, 917–921.
83. Lin, L., Zhou, W., Gao, R., Yao, S., Zhang, X., Xu, W., Zheng, S., Jiang, Z., Yu, Q., Li, Y.W., et al. (2017). Low-temperature hydrogen production from water and methanol using Pt/alpha-MoC catalysts. *Nature* 544, 80–83.
84. Yang, M., Allard, L.F., and Flytzani-Stephanopoulos, M. (2013). Atomically dispersed Au-(OH)<sub>x</sub> species bound on titania catalyze the low-temperature water-gas shift reaction. *J. Am. Chem. Soc.* 135, 3768–3771.
85. Yang, M., Li, S., Wang, Y., Herron, J.A., Xu, Y., Allard, L.F., Lee, S., Huang, J., Mavrikakis, M., and Flytzani-Stephanopoulos, M. (2014). Catalytically active Au-O(OH)<sub>x</sub> species stabilized by alkali ions on zeolites and mesoporous oxides. *Science* 346, 1498–1501.
86. Gai, P.L., Yoshida, K., Ward, M.R., Walsh, M., Baker, R.T., van de Water, L., Watson, M.J., and Boyes, E.D. (2016). Visualisation of single atom dynamics in water-gas shift reaction for hydrogen generation. *Catal. Sci. Technol.* 6, 2214–2227.
87. Ammal, S.C., and Heyden, A. (2017). Water-gas shift activity of atomically dispersed cationic platinum versus metallic platinum clusters on titania supports. *ACS Catal.* 7, 301–309.
88. Li, Q., Ma, Z., Sa, R., Adidharma, H., Gasem, K.A.M., Russell, A.G., Fan, M., and Wu, K. (2017). Computation-predicted, stable, and inexpensive single-atom nanocatalyst Pt@Mo<sub>2</sub>C – an important advanced material for H<sub>2</sub> production. *J. Mater. Chem. A* 5, 14658–14672.
89. Kuai, L., Liu, S., Cao, S., Ren, Y., Kan, E., Zhao, Y., Yu, N., Li, F., Li, X., Wu, Z., et al. (2018). Atomically dispersed Pt/metal oxide mesoporous catalysts from synchronous pyrolysis-deposition route for water-gas shift reaction. *Chem. Mater.* 30, 5534–5538.
90. Yang, M., Liu, J., Lee, S., Zugic, B., Huang, J., Allard, L.F., and Flytzani-Stephanopoulos, M. (2015). A common single-site Pt(II)-O(OH)<sub>x</sub>-species stabilized by sodium on “active” and “inert” supports catalyzes the water-gas shift reaction. *J. Am. Chem. Soc.* 137, 3470–3473.
91. Lin, J., Wang, A., Qiao, B., Liu, X., Yang, X., Wang, X., Liang, J., Li, J., Liu, J., and Zhang, T. (2013). Remarkable performance of Ir<sub>1</sub>/FeO<sub>x</sub> single-atom catalyst in water gas shift reaction. *J. Am. Chem. Soc.* 135, 15314–15317.
92. Sun, X., Lin, J., Zhou, Y., Li, L., Su, Y., Wang, X., and Zhang, T. (2017). FeOx supported

- single-atom Pd bifunctional catalyst for water gas shift reaction. *AIChE J.* 63, 4022–4031.
93. Zeng, M., and Li, Y. (2015). Recent advances in heterogeneous electrocatalysts for the hydrogen evolution reaction. *J. Mater. Chem. A* 3, 14942–14962.
94. Morales-Guio, C.G., Stern, L.A., and Hu, X. (2014). Nanostructured hydrotreating catalysts for electrochemical hydrogen evolution. *Chem. Soc. Rev.* 43, 6555–6569.
95. Seh, Z.W., Kibsgaard, J., Dickens, C.F., Chorkendorff, I., Nørskov, J.K., and Jaramillo, T.F. (2017). Combining theory and experiment in electrocatalysis: insights into materials design. *Science* 355, 1–12.
96. Hossain, M.D., Liu, Z., Zhuang, M., Yan, X., Xu, G.-L., Gadre, C.A., Tyagi, A., Abidi, I.H., Sun, C.-J., Wong, H., et al. (2019). Rational design of graphene-supported single atom catalysts for hydrogen evolution reaction. *Adv. Energy Mater.* 9, 1803689.
97. Zhu, C., Shi, Q., Feng, S., Du, D., and Lin, Y. (2018). Single-atom catalysts for electrochemical water splitting. *ACS Energy Lett.* 3, 1713–1721.
98. Zeng, X., Shui, J., Liu, X., Liu, Q., Li, Y., Shang, J., Zheng, L., and Yu, R. (2018). Single-atom to single-atom grafting of Pt1 onto Fe@N4 center: Pt1@Fe-N-C multifunctional electrocatalyst with significantly enhanced properties. *Adv. Energy Mater.* 8, 1701345.
99. Chao, T., Luo, X., Chen, W., Jiang, B., Ge, J., Lin, Y., Wu, G., Wang, X., Hu, Y., Zhuang, Z., et al. (2017). Atomically dispersed copper-platinum dual sites alloyed with palladium nanorings catalyze the hydrogen evolution reaction. *Angew. Chem. Int. Ed. Engl.* 56, 16047–16051.
100. Liu, D., Li, X., Chen, S., Yan, H., Wang, C., Wu, C., Haleem, Y.A., Duan, S., Lu, J., Ge, B., et al. (2019). Atomically dispersed platinum supported on curved carbon supports for efficient electrocatalytic hydrogen evolution. *Nat. Energy* 4, 512–518.
101. Cao, S., Li, H., Tong, T., Chen, H.-C., Yu, A., Yu, J., and Chen, H.M. (2018). Single-atom engineering of directional charge transfer channels and active sites for photocatalytic hydrogen evolution. *Adv. Funct. Mater.* 28, 1802169.
102. Lu, B., Guo, L., Wu, F., Peng, Y., Lu, J.E., Smart, T.J., Wang, N., Finfrock, Y.Z., Morris, D., Zhang, P., et al. (2019). Ruthenium atomically dispersed in carbon outperforms platinum toward hydrogen evolution in alkaline media. *Nat. Commun.* 10, 631.
103. Wang, D., Li, Q., Han, C., Xing, Z., and Yang, X. (2019). Single-atom ruthenium based catalyst for enhanced hydrogen evolution. *Appl. Catal. B* 249, 91–97.
104. Yuan, S., Pu, Z., Zhou, H., Yu, J., Amiiniu, I.S., Zhu, J., Liang, Q., Yang, J., He, D., Hu, Z., et al. (2019). A universal synthesis strategy for single atom dispersed cobalt/metal clusters heterostructure boosting hydrogen evolution catalysis at all pH values. *Nano Energy* 59, 472–480.
105. Wang, Q., Zhao, Z.L., Dong, S., He, D., Lawrence, M.J., Han, S., Cai, C., Xiang, S., Rodriguez, P., Xiang, B., et al. (2018). Design of active nickel single-atom decorated MoS<sub>2</sub> as a pH-universal catalyst for hydrogen evolution reaction. *Nano Energy* 53, 458–467.
106. Fan, L., Liu, P.F., Yan, X., Gu, L., Yang, Z.Z., Yang, H.G., Qiu, S., and Yao, X. (2016). Atomically isolated nickel species anchored on graphitized carbon for efficient hydrogen evolution electrocatalysis. *Nat. Commun.* 7, 10667.
107. Cheng, N., Stambula, S., Wang, D., Banis, M.N., Liu, J., Riese, A., Xiao, B., Li, R., Sham, T.K., Liu, L.M., et al. (2016). Platinum single-atom and cluster catalysis of the hydrogen evolution reaction. *Nat. Commun.* 7, 13638.
108. Wei, H., Wu, H., Huang, K., Ge, B., Ma, J., Lang, J., Zu, D., Lei, M., Yao, Y., Guo, W., et al. (2019). Ultralow-temperature photochemical synthesis of atomically dispersed Pt catalysts for the hydrogen evolution reaction. *Chem. Sci.* 10, 2830–2836.
109. Yin, X.P., Wang, H.J., Tang, S.F., Lu, X.L., Shu, M., Si, R., and Lu, T.B. (2018). Engineering the coordination environment of single-atom platinum anchored on graphdiyne for optimizing electrocatalytic hydrogen evolution. *Angew. Chem. Int. Ed. Engl.* 57, 9382–9386.
110. Ye, S., Luo, F., Zhang, Q., Zhang, P., Xu, T., Wang, Q., He, D., Guo, L., Zhang, Y., He, C., et al. (2019). Highly stable single Pt atomic sites anchored on aniline-stacked graphene for hydrogen evolution reaction. *Energy Environ. Sci.* 12, 1000–1007.
111. Kwon, H.C., Kim, M., Grote, J.P., Cho, S.J., Chung, M.W., Kim, H., Won, D.H., Zeradjanin, A.R., Mayrhofer, K.J.J., Choi, M., et al. (2018). Carbon monoxide as a promoter of atomically dispersed platinum catalyst in electrochemical hydrogen evolution reaction. *J. Am. Chem. Soc.* 140, 16198–16205.
112. Deng, J., Li, H., Xiao, J., Tu, Y., Deng, D., Yang, H., Tian, H., Li, J., Ren, P., and Bao, X. (2015). Triggering the electrocatalytic hydrogen evolution activity of the inert two-dimensional MoS<sub>2</sub> surface via single-atom metal doping. *Energy Environ. Sci.* 8, 1594–1601.
113. Zhang, L., Jia, Y., Gao, G., Yan, X., Chen, N., Chen, J., Soo, M.T., Wood, B., Yang, D., Du, A., et al. (2018). Graphene defects trap atomic Ni species for hydrogen and oxygen evolution reactions. *Chem* 4, 285–297.
114. Sahoo, S.K., Ye, Y., Lee, S., Park, J., Lee, H., Lee, J., and Han, J.W. (2019). Rational design of TiC-supported single-atom electrocatalysts for hydrogen evolution and selective oxygen reduction reactions. *ACS Energy Lett.* 4, 126–132.
115. Li, Z., Schweitzer, N.M., League, A.B., Bernales, V., Peters, A.W., Getsoiyan, A.B., Wang, T.C., Miller, J.T., Vjunov, A., Fulton, J.L., et al. (2016). Sintering-resistant single-site nickel catalyst supported by metal-organic framework. *J. Am. Chem. Soc.* 138, 1977–1982.
116. Qiu, H.J., Ito, Y., Cong, W., Tan, Y., Liu, P., Hirata, A., Fujita, T., Tang, Z., and Chen, M. (2015). Nanoporous graphene with single-atom nickel dopants: an efficient and stable catalyst for electrochemical hydrogen production. *Angew. Chem. Int. Ed. Engl.* 54, 14031–14035.
117. Cao, L., Luo, Q., Liu, W., Lin, Y., Liu, X., Cao, Y., Zhang, W., Wu, Y., Yang, J., Yao, T., et al. (2019). Identification of single-atom active sites in carbon-based cobalt catalysts during electrocatalytic hydrogen evolution. *Nat. Catal.* 2, 134–141.
118. Tachibana, Y., Vayssieres, L., and Durrant, J.R. (2012). Artificial photosynthesis for solar water-splitting. *Nat. Photonics* 6, 511–518.
119. Ran, J., Zhang, J., Yu, J., Jaroniec, M., and Qiao, S.Z. (2014). Earth-abundant cocatalysts for semiconductor-based photocatalytic water splitting. *Chem. Soc. Rev.* 43, 7787–7812.
120. Song, Q., Li, J., Wang, L., Qin, Y., Pang, L., and Liu, H. (2019). Stable single-atom cobalt as a strong coupling bridge to promote electron transfer and separation in photoelectrocatalysis. *J. Catal.* 370, 176–185.
121. Sui, Y., Liu, S., Li, T., Liu, Q., Jiang, T., Guo, Y., and Luo, J.-L. (2017). Atomically dispersed Pt on specific TiO<sub>2</sub> facets for photocatalytic H<sub>2</sub> evolution. *J. Catal.* 353, 250–255.
122. Trofimovaite, R., Parlett, C.M.A., Kumar, S., Frattini, L., Isaacs, M.A., Wilson, K., Olivi, L., Coulson, B., Debgupta, J., Douthwaite, R.E., et al. (2018). Single atom Cu(I) promoted mesoporous titanias for photocatalytic methyl Orange depollution and H<sub>2</sub> production. *Appl. Catal. B* 232, 501–511.
123. Zhao, Q., Yao, W., Huang, C., Wu, Q., and Xu, Q. (2017). Effective and durable Co single atomic cocatalysts for photocatalytic hydrogen production. *ACS Appl. Mater. Interfaces* 9, 42734–42741.
124. Su, H., Che, W., Tang, F., Cheng, W., Zhao, X., Zhang, H., and Liu, Q. (2018). Valence band engineering via Pt11 single-atom confinement realizing photocatalytic water splitting. *J. Phys. Chem. C* 122, 21108–21114.
125. Li, X., Bi, W., Zhang, L., Tao, S., Chu, W., Zhang, Q., Luo, Y., Wu, C., and Xie, Y. (2016). Single-atom Pt as co-catalyst for enhanced photocatalytic H<sub>2</sub> evolution. *Adv. Mater.* 28, 2427–2431.
126. Fang, X., Shang, Q., Wang, Y., Jiao, L., Yao, T., Li, Y., Zhang, Q., Luo, Y., and Jiang, H.L. (2018). Single Pt atoms confined into a metal-organic framework for efficient photocatalysis. *Adv. Mater.* 30, 29315871.
127. Lee, B.H., Park, S., Kim, M., Sinha, A.K., Lee, S.C., Jung, E., Chang, W.J., Lee, K.S., Kim, J.H., Cho, S.P., et al. (2019). Reversible and cooperative photoactivation of single-atom Cu/TiO<sub>2</sub> photocatalysts. *Nat. Mater.* 18, 620–626.
128. Union of Concerned Scientists. (2018). How Do Hydrogen Fuel Cell Vehicles Work?.
129. Choi, C.H., Kim, M., Kwon, H.C., Cho, S.J., Yun, S., Kim, H.T., Mayrhofer, K.J.J., Kim, H., and Choi, M. (2016). Tuning selectivity of electrochemical reactions by atomically dispersed platinum catalyst. *Nat. Commun.* 7, 10922.
130. Yang, S., Tak, Y.J., Kim, J., Soon, A., and Lee, H. (2017). Support effects in single-atom

- platinum catalysts for electrochemical oxygen reduction. *ACS Catal.* 7, 1301–1307.
131. Liu, J., Jiao, M., Mei, B., Tong, Y., Li, Y., Ruan, M., Song, P., Sun, G., Jiang, L., Wang, Y., et al. (2019). Carbon-supported Divacancy-anchored platinum single-atom electrocatalysts with superhigh Pt utilization for the oxygen reduction reaction. *Angew. Chem. Int. Ed. Engl.* 58, 1163–1167.
132. Zhu, Q.-L., Xia, W., Zheng, L.-R., Zou, R., Liu, Z., and Xu, Q. (2017). Atomically dispersed Fe/N-doped hierarchical carbon architectures derived from a metal–organic framework composite for extremely efficient electrocatalysis. *ACS Energy Lett.* 2, 504–511.
133. Li, Y., Liu, D., Gan, J., Duan, X., Zang, K., Rønning, M., Song, L., Luo, J., and Chen, D. (2019). Sustainable and atomically dispersed iron electrocatalysts derived from nitrogen- and phosphorus-modified woody biomass for efficient oxygen reduction. *Adv. Mater. Interfaces* 6, 1801623.
134. Jiang, R., Li, L., Sheng, T., Hu, G., Chen, Y., and Wang, L. (2018). Edge-site engineering of atomically dispersed Fe-N4 by selective C-N bond cleavage for enhanced oxygen reduction reaction activities. *J. Am. Chem. Soc.* 140, 11594–11598.
135. Wan, G., Yu, P., Chen, H., Wen, J., Sun, C.J., Zhou, H., Zhang, N., Li, Q., Zhao, W., Xie, B., et al. (2018). Engineering single-atom cobalt catalysts toward improved electrocatalysis. *Small* 14, e1704319.
136. Xiao, M., Zhang, H., Chen, Y., Zhu, J., Gao, L., Jin, Z., Ge, J., Jiang, Z., Chen, S., Liu, C., et al. (2018). Identification of binuclear CO<sub>2</sub>N<sub>5</sub> active sites for oxygen reduction reaction with more than one magnitude higher activity than single atom CoN<sub>4</sub> site. *Nano Energy* 46, 396–403.
137. Gong, S., Wang, C., Jiang, P., Hu, L., Lei, H., and Chen, Q. (2018). Designing highly efficient dual-metal single-atom electrocatalysts for the oxygen reduction reaction inspired by biological enzyme systems. *J. Mater. Chem. A* 6, 13254–13262.
138. Li, J., Chen, M., Cullen, D.A., Hwang, S., Wang, M., Li, B., Liu, K., Karakalos, S., Lucero, M., Zhang, H., et al. (2018). Atomically dispersed manganese catalysts for oxygen reduction in proton-exchange membrane fuel cells. *Nat. Catal.* 1, 935–945.
139. Li, F., Han, G.-F., Noh, H.-J., Kim, S.-J., Lu, Y., Jeong, H.Y., Fu, Z., and Baek, J.-B. (2018). Boosting oxygen reduction catalysis with abundant copper single atom active sites. *Energy Environ. Sci.* 11, 2263–2269.
140. Song, P., Luo, M., Liu, X., Xing, W., Xu, W., Jiang, Z., and Gu, L. (2017). Zn single atom catalyst for highly efficient oxygen reduction reaction. *Adv. Funct. Mater.* 27, 1700802.
141. Xiao, M., Zhu, J., Ma, L., Jin, Z., Ge, J., Deng, X., Hou, Y., He, Q., Li, J., Jia, Q., et al. (2018). Microporous framework induced synthesis of single-atom dispersed Fe-N-C acidic ORR catalyst and its in situ reduced Fe-N<sub>4</sub> active site identification revealed by X-ray absorption spectroscopy. *ACS Catal.* 8, 2824–2832.
142. Lai, W.H., Zhang, B.W., Hu, Z., Qu, X.M., Jiang, Y.X., Wang, Y.X., Wang, J.Z., Liu, H.K., and Chou, S.L. (2019). The quasi-Pt-allotrope catalyst: hollow PtCo@single-Atom Pt1 on nitrogen-doped carbon toward superior oxygen reduction. *Adv. Funct. Mater.* 1, 29.
143. Zhang, C., Sha, J., Fei, H., Liu, M., Yazdi, S., Zhang, J., Zhong, Q., Zou, X., Zhao, N., Yu, H., et al. (2017). Single-atomic ruthenium catalytic sites on nitrogen-doped graphene for oxygen reduction reaction in acidic medium. *ACS Nano* 11, 6930–6941.
144. Zhu, C., Fu, S., Song, J., Shi, Q., Su, D., Engelhard, M.H., Li, X., Xiao, D., Li, D., Estevez, L., et al. (2017). Self-assembled Fe-N-doped carbon nanotube aerogels with single-atom catalyst feature as high-efficiency oxygen reduction electrocatalysts. *Small* 13, 28165196.
145. Jiao, L., Wan, G., Zhang, R., Zhou, H., Yu, S.H., and Jiang, H.L. (2018). From metal–organic frameworks to single-atom Fe implanted N-doped porous carbons: efficient oxygen reduction in both alkaline and acidic media. *Angew. Chem. Int. Ed. Engl.* 57, 8525–8529.
146. Wang, J., Han, G., Wang, L., Du, L., Chen, G., Gao, Y., Ma, Y., Du, C., Cheng, X., Zuo, P., et al. (2018). ZIF-8 with ferrocene encapsulated: a promising precursor to single-atom Fe embedded nitrogen-doped carbon as highly efficient catalyst for oxygen electroreduction. *Small* 14, e1704282.
147. Chen, Y., Li, Z., Zhu, Y., Sun, D., Liu, X., Xu, L., and Tang, Y. (2019). Atomic Fe dispersed on N-doped carbon hollow nanospheres for high-efficiency electrocatalytic oxygen reduction. *Adv. Mater.* 31, e1806312.
148. Sun, T., Zhao, S., Chen, W., Zhai, D., Dong, J., Wang, Y., Zhang, S., Han, A., Gu, L., Yu, R., et al. (2018). Single-atomic cobalt sites embedded in hierarchically ordered porous nitrogen-doped carbon as a superior bifunctional electrocatalyst. *Proc. Natl. Acad. Sci. USA* 115, 12692–12697.
149. Han, Y., Wang, Y.G., Chen, W., Xu, R., Zheng, L., Zhang, J., Luo, J., Shen, R.A., Zhu, Y., Cheong, W.C., et al. (2017). Hollow N-doped carbon spheres with isolated cobalt single atomic sites: superior electrocatalysts for oxygen reduction. *J. Am. Chem. Soc.* 139, 17269–17272.
150. Zhu, C., Shi, Q., Xu, B.Z., Fu, S., Wan, G., Yang, C., Yao, S., Song, J., Zhou, H., Du, D., et al. (2018). Hierarchically porous M-N-C (M = Co and Fe) single-atom electrocatalysts with robust MNx active moieties enable enhanced ORR performance. *Adv. Energy Mater.* 8, 1801956.
151. Qiu, X., Yan, X., Pang, H., Wang, J., Sun, D., Wei, S., Xu, L., and Tang, Y. (2019). Isolated Fe single atomic sites anchored on highly steady hollow graphene nanospheres as an efficient electrocatalyst for the oxygen reduction reaction. *Adv. Sci.* 6, 1801103.
152. Shen, H., Gracia-Espino, E., Ma, J., Zang, K., Luo, J., Wang, L., Gao, S., Mamat, X., Hu, G., Wagberg, T., et al. (2017). Synergistic effects between atomically dispersed Fe-N-C and C-S-C for the oxygen reduction reaction in acidic media. *Angew. Chem. Int. Ed. Engl.* 56, 13800–13804.
153. Zitolo, A., Goellner, V., Armel, V., Sougrati, M.T., Mineva, T., Stievano, L., Fonda, E., and Jaouen, F. (2015). Identification of catalytic sites for oxygen reduction in iron- and nitrogen-doped graphene materials. *Nat. Mater.* 14, 937–942.
154. Yang, L., Cheng, D., Xu, H., Zeng, X., Wan, X., Shui, J., Xiang, Z., and Cao, D. (2018). Unveiling the high-activity origin of single-atom iron catalysts for oxygen reduction reaction. *Proc. Natl. Acad. Sci. USA* 115, 6626–6631.
155. Zhang, H., Hwang, S., Wang, M., Feng, Z., Karakalos, S., Luo, L., Qiao, Z., Xie, X., Wang, C., Su, D., et al. (2017). Single atomic iron catalysts for oxygen reduction in acidic media: particle size control and thermal activation. *J. Am. Chem. Soc.* 139, 14143–14149.
156. Gao, Y., Cai, Z., Wu, X., Lv, Z., Wu, P., and Cai, C. (2018). Graphdiyne-supported single-atom-sized Fe catalysts for the oxygen reduction reaction: DFT predictions and experimental validations. *ACS Catal.* 8, 10364–10374.
157. Liu, J., Jiao, M., Lu, L., Barkholtz, H.M., Li, Y., Wang, Y., Jiang, L., Wu, Z., Liu, D.J., Zhuang, L., et al. (2017). High performance platinum single atom electrocatalyst for oxygen reduction reaction. *Nat. Commun.* 8, 15938.
158. Yang, Z., Wang, Y., Zhu, M., Li, Z., Chen, W., Wei, W., Yuan, T., Qu, Y., Xu, Q., Zhao, C., et al. (2019). Boosting oxygen reduction catalysis with Fe-N<sub>2</sub> sites decorated porous carbons toward fuel cells. *ACS Catal.* 9, 2158–2163.
159. Chen, Y., Ji, S., Zhao, S., Chen, W., Dong, J., Cheong, W.C., Shen, R., Wen, X., Zheng, L., Rykov, A.I., et al. (2018). Enhanced oxygen reduction with single-atomic-site iron catalysts for a zinc-air battery and hydrogen-air fuel cell. *Nat. Commun.* 9, 5422.
160. Yang, Z.K., Yuan, C.Z., and Xu, A.W. (2018). A rationally designed Fe-tetrapyridophenazine complex: a promising precursor to a single-atom Fe catalyst for an efficient oxygen reduction reaction in high-power Zn-air cells. *Nanoscale* 10, 16145–16152.
161. Wei, Q., Zhang, G., Yang, X., Fu, Y., Yang, G., Chen, N., Chen, W., and Sun, S. (2018). Litchi-like porous Fe/N/C spheres with atomically dispersed FeNx promoted by sulfur as highly efficient oxygen electrocatalysts for Zn-air batteries. *J. Mater. Chem. A* 6, 4605–4610.
162. Jia, N., Xu, Q., Zhao, F., Gao, H.-X., Song, J., Chen, P., An, Z., Chen, X., and Chen, Y. (2018). Fe/N codoped carbon nanocages with single-atom feature as efficient oxygen reduction reaction electrocatalyst. *ACS Appl. Energy Mater.* 1, 4982–4990.
163. Pan, Y., Liu, S., Sun, K., Chen, X., Wang, B., Wu, K., Cao, X., Cheong, W.C., Shen, R., Han, A., et al. (2018). A bimetallic Zn/Fe polyphthalocyanine-derived single-atom Fe-N4 catalytic site: A superior trifunctional catalyst for overall water splitting and Zn-air batteries. *Angew. Chem. Int. Ed. Engl.* 57, 8614–8618.
164. Chen, P., Zhou, T., Xing, L., Xu, K., Tong, Y., Xie, H., Zhang, L., Yan, W., Chu, W., Wu, C., et al. (2017). Atomically dispersed

- iron-nitrogen species as electrocatalysts for bifunctional oxygen evolution and reduction reactions. *Angew. Chem. Int. Ed. Engl.* 56, 610–614.
165. Yang, L., Shi, L., Wang, D., Lv, Y., and Cao, D. (2018). Single-atom cobalt electrocatalysts for foldable solid-state Zn-air battery. *Nano Energy* 50, 691–698.
166. Han, X., Ling, X., Wang, Y., Ma, T., Zhong, C., Hu, W., and Deng, Y. (2019). Generation of nanoparticle, atomic-cluster, and single-atom cobalt catalysts from zeolitic imidazole frameworks by spatial isolation and their use in zinc-air batteries. *Angew. Chem. Int. Ed. Engl.* 58, 5359–5364.
167. Cheng, C., Li, S., Xia, Y., Ma, L., Nie, C., Roth, C., Thomas, A., and Haag, R. (2018). Atomic Fe-Nx coupled open-mesoporous carbon nanofibers for efficient and bioadaptable oxygen electrode in Mg-air batteries. *Adv. Mater.* e1802669.
168. Du, Z., Chen, X., Hu, W., Chuang, C., Xie, S., Hu, A., Yan, W., Kong, X., Wu, X., Ji, H., et al. (2019). Cobalt in nitrogen-doped graphene as single-atom catalyst for high-sulfur content lithium-sulfur batteries. *J. Am. Chem. Soc.* 141, 3977–3985.
169. Zhou, F., Azofra, L.M., Ali, M., Kar, M., Simonov, A.N., McDonnell-Worth, C., Sun, C., Zhang, X., and MacFarlane, D.R. (2017). Electro-synthesis of ammonia from nitrogen at ambient temperature and pressure in ionic liquids. *Energy Environ. Sci.* 10, 2516–2520.
170. Martín, A.J., Shinagawa, T., and Pérez-Ramírez, J. (2019). Electrocatalytic reduction of nitrogen: From haber-Bosch to ammonia artificial leaf. *Chem* 5, 263–283.
171. Suryanto, B.H.R., Du, H.-L., Wang, D., Chen, J., Simonov, A.N., and MacFarlane, D.R. (2019). Challenges and prospects in the catalysis of electroreduction of nitrogen to ammonia. *Nat. Catal.* 2, 290–296.
172. Ma, X.L., Liu, J.C., Xiao, H., and Li, J. (2018). Surface single-cluster catalyst for N<sub>2</sub>-to-NH<sub>3</sub> thermal conversion. *J. Am. Chem. Soc.* 140, 46–49.
173. Wang, Y., Cui, X., Zhao, J., Jia, G., Gu, L., Zhang, Q., Meng, L., Shi, Z., Zheng, L., Wang, C., et al. (2019). Rational design of Fe-N/C hybrid for enhanced nitrogen reduction electrocatalysis under ambient conditions in aqueous solution. *ACS Catal.* 9, 336–344.
174. Geng, Z., Liu, Y., Kong, X., Li, P., Li, K., Liu, Z., Du, J., Shu, M., Si, R., and Zeng, J. (2018). Achieving a record-high yield rate of 120.9 for N<sub>2</sub> electrochemical reduction over Ru single-atom catalysts. *Adv. Mater.* 30, 1803498.
175. Tao, H., Choi, C., Ding, L.-X., Jiang, Z., Han, Z., Jia, M., Fan, Q., Gao, Y., Wang, H., Robertson, A.W., et al. (2019). Nitrogen fixation by Ru single-atom electrocatalytic reduction. *Chem* 5, 204–214.
176. Cao, Y., Gao, Y., Zhou, H., Chen, X., Hu, H., Deng, S., Zhong, X., Zhuang, G., and Wang, J. (2018). Highly efficient ammonia synthesis electrocatalyst: single Ru atom on naturally nanoporous carbon materials. *Adv. Theory Simul.* 1, 1800018.
177. Zhao, W., Zhang, L., Luo, Q., Hu, Z., Zhang, W., Smith, S., and Yang, J. (2019). Single Mo<sub>1</sub>(Cr<sub>1</sub>) atom on nitrogen-doped graphene enables highly selective electroreduction of nitrogen into ammonia. *ACS Catal.* 9, 3419–3425.
178. Zhao, J., and Chen, Z. (2017). Single Mo atom supported on defective boron nitride monolayer as an efficient electrocatalyst for nitrogen fixation: a computational study. *J. Am. Chem. Soc.* 139, 12480–12487.
179. Choi, C., Back, S., Kim, N.-Y., Lim, J., Kim, Y.-H., and Jung, Y. (2018). Suppression of hydrogen evolution reaction in electrochemical N<sub>2</sub> reduction using single-atom catalysts: a computational guideline. *ACS Catal.* 8, 7517–7525.
180. Zhang, N., Jalil, A., Wu, D., Chen, S., Liu, Y., Gao, C., Ye, W., Qi, Z., Ju, H., Wang, C., et al. (2018). Refining defect states in W<sub>18</sub>O<sub>49</sub> by Mo doping: a strategy for tuning N<sub>2</sub> activation towards solar-driven nitrogen fixation. *J. Am. Chem. Soc.* 140, 9434–9443.
181. Ling, C., Niu, X., Li, Q., Du, A., and Wang, J. (2018). Metal-free single atom catalyst for N<sub>2</sub> fixation driven by visible light. *J. Am. Chem. Soc.* 140, 14161–14168.
182. Energy, U.S.D.o. (2015) Process Intensification Workshop.
183. Lab, O.R.N. (2005). Materials for Separation Technologies. Energy and Emission Reduction Opportunities (Oak Ridge).
184. Humphrey, J.L., and Siebert, A.F. (1992). New horizons in distillation. *Chem. Eng.* 86–98.
185. Pei, G.X., Liu, X.Y., Wang, A., Lee, A.F., Isaacs, M.A., Li, L., Pan, X., Yang, X., Wang, X., Tai, Z., et al. (2015). Ag alloyed Pd single-atom catalysts for efficient selective hydrogenation of acetylene to ethylene in excess ethylene. *ACS Catal.* 5, 3717–3725.
186. Vilé, G., Albani, D., Nachtegaal, M., Chen, Z., Dontsova, D., Antonietti, M., López, N., and Pérez-Ramírez, J. (2015). A stable single-site palladium catalyst for hydrogenations. *Angew. Chem. Int. Ed. Engl.* 54, 11265–11269.
187. Kyriakou, G., Boucher, M.B., Jewell, A.D., Lewis, E.A., Lawton, T.J., Baber, A.E., Tierney, H.L., Flytzani-Stephanopoulos, M., and Sykes, E.C.H. (2012). Isolated metal atom geometries as a strategy for selective heterogeneous hydrogenations. *Science* 335, 1209–1212.
188. Yan, H., Cheng, H., Yi, H., Lin, Y., Yao, T., Wang, C., Li, J., Wei, S., and Lu, J. (2015). Single-atom Pd<sub>1</sub>/graphene catalyst achieved by atomic layer deposition: remarkable performance in selective hydrogenation of 1,3-butadiene. *J. Am. Chem. Soc.* 137, 10484–10487.
189. Huang, X., Xia, Y., Cao, Y., Zheng, X., Pan, H., Zhu, J., Ma, C., Wang, H., Li, J., You, R., et al. (2017). Enhancing both selectivity and coking-resistance of a single-atom Pd<sub>1</sub>/C<sub>7</sub>N<sub>4</sub> catalyst for acetylene hydrogenation. *Nano Res.* 10, 1302–1312.
190. Liu, P., Zhao, Y., Qin, R., Mo, S., Chen, G., Gu, L., Chevrier, D.M., Zhang, P., Guo, Q., Zang, D., et al. (2016). Photochemical route for synthesizing atomically dispersed palladium catalysts. *Science* 352, 797–801.
191. Zhang, B., Asakura, H., Zhang, J., Zhang, J., De, S., and Yan, N. (2016). Stabilizing a platinum single-atom catalyst on supported phosphomolybdic acid without compromising hydrogenation activity. *Angew. Chem. Int. Ed. Engl.* 55, 8319–8323.
192. Lucci, F.R., Liu, J., Marcinkowski, M.D., Yang, M., Allard, L.F., Flytzani-Stephanopoulos, M., and Sykes, E.C.H. (2015). Selective hydrogenation of 1,3-butadiene on platinum–copper alloys at the single-atom limit. *Nat. Commun.* 6, 8550.
193. Zhang, Z., Zhu, Y., Asakura, H., Zhang, B., Zhang, J., Zhou, M., Han, Y., Tanaka, T., Wang, A., Zhang, T., et al. (2017). Thermally stable single atom Pt/m-Al<sub>2</sub>O<sub>3</sub> for selective hydrogenation and CO oxidation. *Nat. Commun.* 8, 16100.
194. Zhang, B., Sun, G., Ding, S., Asakura, H., Zhang, J., Sautet, P., and Yan, N. (2019). Atomically dispersed Pt<sub>1</sub>-Polyoxometalate Catalysts: How Does Metal-Support Interaction Affect Stability and Hydrogenation Activity? *J. Am. Chem. Soc.* 141, 8185–8197.
195. Lin, R., Albani, D., Fako, E., Kaiser, S.K., Safonova, O.V., López, N., and Pérez-Ramírez, J. (2019). Design of single gold atoms on nitrogen-doped carbon for molecular recognition in alkyne semi-hydrogenation. *Angew. Chem. Int. Ed. Engl.* 58, 504–509.
196. Wei, H., Liu, X., Wang, A., Zhang, L., Qiao, B., Yang, X., Huang, Y., Miao, S., Liu, J., and Zhang, T. (2014). FeO<sub>x</sub>-supported platinum single-atom and pseudo-single-atom catalysts for chemoselective hydrogenation of functionalized nitroarenes. *Nat. Commun.* 5, 5634.
197. Wang, L., Guan, E., Zhang, J., Yang, J., Zhu, Y., Han, Y., Yang, M., Cen, C., Fu, G., Gates, B.C., et al. (2018). Single-site catalyst promoters accelerate metal-catalyzed nitroarene hydrogenation. *Nat. Commun.* 9, 1362.
198. Liu, W., Zhang, L., Yan, W., Liu, X., Yang, X., Miao, S., Wang, W., Wang, A., and Zhang, T. (2016). Single-atom dispersed Co–N–C catalyst: structure identification and performance for hydrogenative coupling of nitroarenes. *Chem. Sci.* 7, 5758–5764.
199. Yan, H., Zhao, X., Guo, N., Lyu, Z., Du, Y., Xi, S., Guo, R., Chen, C., Chen, Z., Liu, W., et al. (2018). Atomic engineering of high-density isolated Co atoms on graphene with proximal-atom controlled reaction selectivity. *Nat. Commun.* 9, 3197.
200. Wang, X., Chen, W., Zhang, L., Yao, T., Liu, W., Lin, Y., Ju, H., Dong, J., Zheng, L., Yan, W., et al. (2017). Uncoordinated amine groups of metal–organic frameworks to anchor single Ru sites as chemoselective catalysts toward the hydrogenation of quinoline. *J. Am. Chem. Soc.* 139, 9419–9422.
201. Lin, L., Yao, S., Gao, R., Liang, X., Yu, Q., Deng, Y., Liu, J., Peng, M., Jiang, Z., Li, S., et al. (2019). A highly CO-tolerant atomically dispersed Pt catalyst for chemoselective hydrogenation. *Nat. Nanotechnol.* 14, 354–361.
202. Liu, J., Lucci, F.R., Yang, M., Lee, S., Marcinkowski, M.D., Therrien, A.J., Williams, C.T., Sykes, E.C.H., and

- Flytzani-Stephanopoulos, M. (2016). Tackling CO poisoning with single-atom alloy catalysts. *J. Am. Chem. Soc.* 138, 6396–6399.
203. Chen, Y., Lin, J., Li, L., Qiao, B., Liu, J., Su, Y., and Wang, X. (2018). Identifying size effects of Pt as single atoms and nanoparticles supported on FeOx for the water-gas shift reaction. *ACS Catal.* 8, 859–868.
204. Nie, L., Mei, D., Xiong, H., Peng, B., Ren, Z., Hernandez, X.I.P., DelaRiva, A., Wang, M., Engelhard, M.H., Kovarik, L., et al. (2017). Activation of surface lattice oxygen in single-atom Pt/CeO<sub>2</sub> for low-temperature CO oxidation. *Science* 358, 1419–1423.
205. Pereira-Hernández, X.I., DelaRiva, A., Muravev, V., Kunwar, D., Xiong, H., Sudduth, B., Engelhard, M., Kovarik, L., Hensen, E.J.M., Wang, Y., et al. (2019). Tuning Pt-CeO<sub>2</sub> interactions by high-temperature vapor-phase synthesis for improved reducibility of lattice oxygen. *Nat. Commun.* 10, 1358.
206. Lang, R., Li, T., Matsumura, D., Miao, S., Ren, Y., Cui, Y.-T., Tan, Y., Qiao, B., Li, L., Wang, A., et al. (2016). Hydroformylation of olefins by a rhodium single-atom catalyst with activity comparable to RhCl(PPh<sub>3</sub>)<sub>3</sub>. *Angew. Chem. Int. Ed.* 128, 16288–16292.
207. Wang, L., Zhang, W., Wang, S., Gao, Z., Luo, Z., Wang, X., Zeng, R., Li, A., Li, H., Wang, M., et al. (2016). Atomic-level insights in optimizing reaction paths for hydroformylation reaction over Rh/CoO single-atom catalyst. *Nat. Commun.* 7, 14036.
208. Cui, X., Junge, K., Dai, X., Kreyenschulte, C., Pohl, M.M., Wohlrab, S., Shi, F., Brückner, A., and Beller, M. (2017). Synthesis of single atom based heterogeneous platinum catalysts: high selectivity and activity for hydrosilylation reactions. *ACS Cent. Sci.* 3, 580–585.
209. Zhu, Y., Cao, T., Cao, C., Luo, J., Chen, W., Zheng, L., Dong, J., Zhang, J., Han, Y., Li, Z., et al. (2018). One-Pot pyrolysis to N-doped graphene with high-density Pt single atomic sites as heterogeneous catalyst for alkene hydrosilylation. *ACS Catal.* 8, 10004–10011.
210. Chen, Y., Ji, S., Sun, W., Chen, W., Dong, J., Wen, J., Zhang, J., Li, Z., Zheng, L., Chen, C., et al. (2018). Discovering partially charged single-atom Pt for enhanced anti-Markovnikov alkene hydrosilylation. *J. Am. Chem. Soc.* 140, 7407–7410.
211. Miura, H., Endo, K., Ogawa, R., and Shishido, T. (2017). Supported palladium–gold alloy catalysts for efficient and selective hydrosilylation under mild conditions with isolated single palladium atoms in alloy nanoparticles as the main active site. *ACS Catal.* 7, 1543–1553.
212. Malta, G., Kondrat, S.A., Freakley, S.J., Davies, C.J., Lu, L., Dawson, S., Thetford, A., Gibson, E.K., Morgan, D.J., Jones, W., et al. (2017). Identification of single-site gold catalysis in acetylene hydrochlorination. *Science* 355, 1399–1403.
213. Kaiser, S.K., Lin, R., Mitchell, S., Fako, E., Krumeich, F., Hauer, R., Safonova, O.V., Kondratenko, V.A., Kondratenko, E.V., Collins, S.M., et al. (2019). Controlling the speciation and reactivity of carbon-supported gold nanostructures for catalysed acetylene hydrochlorination. *Chem. Sci.* 10, 359–369.
214. Ye, L., Duan, X., Wu, S., Wu, T.S., Zhao, Y., Robertson, A.W., Chou, H.L., Zheng, J., Ayvali, T., Day, S., et al. (2019). Self-regeneration of Au/CeO<sub>2</sub> based catalysts with enhanced activity and ultra-stability for acetylene hydrochlorination. *Nat. Commun.* 10, 914.
215. Zhang, L., Wang, A., Miller, J.T., Liu, X., Yang, X., Wang, W., Li, L., Huang, Y., Mou, C.-Y., and Zhang, T. (2014). Efficient and durable Au alloyed Pd single-atom catalyst for the Ullmann reaction of aryl chlorides in water. *ACS Catal.* 4, 1546–1553.
216. Fernández, E., Rivero-Crespo, M.A., Domínguez, I., Rubio-Marqués, P., Oliver-Meseguer, J., Liu, L., Cabrer-Antón, M., Gavara, R., Hernández-Garrido, J.C., Boronat, M., et al. (2019). Base-controlled Heck, Suzuki, and Sonogashira reactions catalyzed by ligand-free platinum or palladium single atom and sub-nanometer clusters. *J. Am. Chem. Soc.* 141, 1928–1940.
217. Zhang, X., Sun, Z., Wang, B., Tang, Y., Nguyen, L., Li, Y., and Tao, F.F. (2018). C–C coupling on single-atom-based heterogeneous catalyst. *J. Am. Chem. Soc.* 140, 954–962.
218. Lee, E.-K., Park, S.-A., Woo, H., Hyun Park, K., Kang, D.W., Lim, H., and Kim, Y.-T. (2017). Platinum single atoms dispersed on carbon nanotubes as reusable catalyst for Suzuki coupling reaction. *J. Catal.* 352, 388–393.
219. Chen, Z., Vorobyeva, E., Mitchell, S., Fako, E., Ortuño, M.A., López, N., Collins, S.M., Midgley, P.A., Richard, S., Vilé, G., et al. (2018). A heterogeneous single-atom palladium catalyst surpassing homogeneous systems for Suzuki coupling. *Nat. Nanotechnol.* 13, 702–707.
220. Xiong, H., Lin, S., Goetze, J., Pletcher, P., Guo, H., Kovarik, L., Artyushkova, K., Weckhuysen, B.M., and Datye, A.K. (2017). Thermally stable and regenerable platinum–tin clusters for propane dehydrogenation prepared by atom trapping on ceria. *Angew. Chem. Int. Ed. Engl.* 56, 8986–8991.
221. Sun, G., Zhao, Z.J., Mu, R., Zha, S., Li, L., Chen, S., Zang, K., Luo, J., Li, Z., Purdy, S.C., et al. (2018). Breaking the scaling relationship via thermally stable Pt/Cu single atom alloys for catalytic dehydrogenation. *Nat. Commun.* 9, 4454.
222. Cao, X., Ji, Y., and Luo, Y. (2015). Dehydrogenation of propane to propylene by a Pd/Cu single-atom catalyst: insight from first-principles calculations. *J. Phys. Chem. C* 119, 1016–1023.
223. Kim, Y.-T., Ohshima, K., Higashimine, K., Uruga, T., Takata, M., Suematsu, H., and Mitani, T. (2006). Fine size control of platinum on carbon nanotubes: From single atoms to clusters. *Angew. Chem. Int. Ed.* 118, 421–425.
224. von Weber, A., Baxter, E.T., Proch, S., Kane, M.D., Rosenfelder, M., White, H.S., and Anderson, S.L. (2015). Size-dependent electronic structure controls activity for ethanol electro-oxidation at Pt<sub>n</sub>/indium tin oxide ( $n = 1$  to 14). *Phys. Chem. Chem. Phys.* 17, 17601–17610.
225. Liu, R., Zhang, L.Q., Yu, C., Sun, M.T., Liu, J.F., and Jiang, G.B. (2017). Atomic-level-designed catalytically active palladium atoms on ultrathin gold nanowires. *Adv. Mater.* 29, adma.201604571.
226. Goodman, E.D., Johnston-Peck, A.C., Dietze, E.M., Wrasman, C.J., Hoffman, A.S., Abild-Pedersen, F., Bare, S.R., Plessow, P.N., and Cargnello, M. (2019). Catalyst deactivation via decomposition into single atoms and the role of metal loading. *Nat. Catal.* 2, 748–755.
227. Dahl, S., Logadottir, A., Egeberg, R.C., Larsen, J.H., Chorkendorff, I., Törnqvist, E., and Nørskov, J.K. (1999). Role of steps in N<sub>2</sub> activation on Ru(0001). *Phys. Rev. Lett.* 83, 1814–1817.
228. Hülsey, M.J., Zhang, J., and Yan, N. (2018). Harnessing the wisdom in colloidal chemistry to make stable single-atom catalysts. *Adv. Mater.* 30, e1802304.
229. Ertl, G., Knoezinger, H., Schuetz, F., and Weitkamp, J. (1999). *Handbook of Heterogeneous Catalysis* (John Wiley and Sons, Inc.).
230. Yao, Y., Huang, Z., Xie, P., Wu, L., Ma, L., Li, T., Pang, Z., Jiao, M., Liang, Z., Gao, J., et al. (2019). High temperature shockwave stabilized single atoms. *Nat. Nanotechnol.* 14, 851–857.
231. Lin, Y.C., Teng, P.Y., Chiu, P.W., and Suenaga, K. (2015). Exploring the single atom spin state by electron spectroscopy. *Phys. Rev. Lett.* 115, 206803.
232. Mecklenburg, M., Hubbard, W.A., White, E.R., Dhall, R., Cronin, S.B., Aloni, S., and Regan, B.C. (2015). Thermal measurement. Nanoscale temperature mapping in operating microelectronic devices. *Science* 347, 629–632.
233. Lagos, M.J., and Batson, P.E. (2018). Thermometry with subnanometer resolution in the electron microscope using the principle of detailed balancing. *Nano Lett.* 18, 4556–4563.
234. Marcinkowski, M.D., Darby, M.T., Liu, J., Wimble, J.M., Lucci, F.R., Lee, S., Michaelides, A., Flytzani-Stephanopoulos, M., Stamatakis, M., and Sykes, E.C.H. (2018). Pt/Cu single-atom alloys as coke-resistant catalysts for efficient C–H activation. *Nat. Chem.* 10, 325–332.
235. Chen, X., Engle, K.M., Wang, D.H., and Yu, J.Q. (2009). Palladium(II)-catalyzed C–H activation/C–C cross-coupling reactions: versatility and practicality. *Angew. Chem. Int. Ed. Engl.* 48, 5094–5115.
236. McCrory, C.C., Jung, S., Peters, J.C., and Jaramillo, T.F. (2013). Benchmarking heterogeneous electrocatalysts for the oxygen evolution reaction. *J. Am. Chem. Soc.* 135, 16977–16987.
237. Spöri, C., Kwan, J.T.H., Bonakdarpour, A., Wilkinson, D.P., and Strasser, P. (2017). The stability challenges of oxygen evolving catalysts: towards a common fundamental understanding and mitigation of catalyst degradation. *Angew. Chem. Int. Ed. Engl.* 56, 5994–6021.

238. Grajciar, L., Heard, C.J., Bondarenko, A.A., Polynski, M.V., Meeprasert, J., Pidko, E.A., and Nachtigall, P. (2018). Towards operando computational modeling in heterogeneous catalysis. *Chem. Soc. Rev.* 47, 8307–8348.
239. Sun, M., Wu, T., Xue, Y., Dougherty, A.W., Huang, B., Li, Y., and Yan, C.-H. (2019). Mapping of atomic catalyst on graphdiyne. *Nano Energy* 62, 754–763.
240. Vorobyeva, E., Fako, E., Chen, Z., Collins, S.M., Johnstone, D., Midgley, P.A., Hauert, R., Safonova, O.V., Vilé, G., López, N., et al. (2019). Atom-by-atom resolution of structure-function relations over low-nuclearity metal catalysts. *Angew. Chem. Int. Ed. Engl.* 58, 8724–8729.
241. Zhao, Y., Yang, K.R., Wang, Z., Yan, X., Cao, S., Ye, Y., Dong, Q., Zhang, X., Thorne, J.E., Jin, L., et al. (2018). Stable iridium dinuclear heterogeneous catalysts supported on metal-oxide substrate for solar water oxidation. *Proc. Natl. Acad. Sci. USA* 115, 2902–2907.
242. Yan, H., Lin, Y., Wu, H., Zhang, W., Sun, Z., Cheng, H., Liu, W., Wang, C., Li, J., Huang, X., et al. (2017). Bottom-up precise synthesis of stable platinum dimers on graphene. *Nat. Commun.* 8, 1070.
243. Liu, J.C., Ma, X.L., Li, Y., Wang, Y.G., Xiao, H., and Li, J. (2018). Heterogeneous Fe<sub>3</sub> single-cluster catalyst for ammonia synthesis via an associative mechanism. *Nat. Commun.* 9, 1610.
244. Liu, C., Li, Q., Wu, C., Zhang, J., Jin, Y., MacFarlane, D.R., and Sun, C. (2019). Single-boron catalysts for nitrogen reduction reaction. *J. Am. Chem. Soc.* 141, 2884–2888.